CONTRACT REPORT NO. 3-118

PHOTOELASTIC STUDIES FOR VEHICLE MOBILITY RESEARCH

by

F. M. Mellinger

J. H. Hubbard

R. L. Peters

August 1965

Sponsored by

Directorate of Research and Development

U. S. Army Materiel Command

Conducted for

U. S. Army Engineer Waterways Experiment Station

CORPS OF ENGINEERS

Vicksburg, Mississippi

by

U. S. Army Engineer Division

Ohio River

Ohio River Division Laboratories

Cincinnati, Ohio

CONTRACT REPORT NO. 3-118

PHOTOELASTIC STUDIES FOR VEHICLE MOBILITY RESEARCH

by

F. M. Mellinger
J. H. Hubbard
R. L. Peters

August 1965

Sponsored by

Directorate of Research and Development
U. S. Army Materiel Command
Project No. 1-V-0-21701-A-046-03

Conducted for

U. S. Army Engineer Waterways Experiment Station
CORPS OF ENGINEERS
Vicksburg, Mississippi

by

U. S. Army Engineer Division
Ohio River
Ohio River Division Laboratories
Cincinnati, Ohio

PREFACE

The investigation reported herein was conducted in accord with the request contained in letter from the U. S. Army waterways Experiment Station to the Ohio River Division Laboratories subject, "Photoelastic Studies for Vehicle Mobility Research" dated 3 January 1964, and indorsements thereon. The study was part of the research being conducted under DA Project 1-V-0-21701-A-046, "Trafficability and Mobility Research," Task 1-V-0-21701-A-046-03, "Mobility Fundamentals and Model Studies," under the sponsorship and guidance of the Directorate of Research and Development, U. S. Army Materiel Command.

These studies, which were conducted by the U. S. Army Engineer Division, Ohio River, Ohio River Division Laboratories (ORDL), included investigations of the mode of failure of gelatin under the influence of various probe shapes, and the qualitative investigations of the state of stress within the gelatin as affected by a moving wheel load with controlled slip. Laboratory tests to determine the strength characteristics of gelatin also were performed there.

ORDL personnel actively engaged with the planning, testing, analysis, and report phases of the work were Messrs. F. M. Mellinger, R. L. Hutchinson, J. H. Hubbard, R. L. Peters, and D. J. Calvert. Principal contact personnel at the WES were Messrs. G. W. Turnage, C. J. Powell, and D. R. Freitag of the Mobility Section, Army Mobility Research Branch, Mobility and Environmental Division. This report was prepared by Messrs. F. M. Mellinger, J. H. Hubbard, and R. L. Peters, all of ORDL. Messrs. F. M. Mellinger and J. M. Merzweiler were Director and Assistant Director, respectively, of the Ohio River Division Laboratories during this study.

CONTENTS

CONTENTS (Cont'd)

SUMMARY

The test procedures and techniques developed in the studies reported herein provide a means of obtaining photoelastic stress patterns for moving wheel loads at controlled degrees of slip. Sufficient information was developed to compute normal and shear stress distribution on planes in the gelatin foundation within one-fourth inch of the contact surface between the moving wheel load and gelatin, if certain approximations are made. Further study is indicated to accurately define the stress at a point.

Concerning the action of the static and moving wheel loads on the gelatin model, it was found that there was an increase in maximum shear stress for the moving wheel load at 0, +25%, and +50% slip over that of an equivalent static wheel load. This increase in maximum shear stress was due to a redistribution of normal stress at the wheel contact with the gelatin. Also, the maximum shear stress under the action of the moving wheel load was greater at 0 slip than at +25% and +50% slip.

PHOTOELASTIC STUDIES FOR VEHICLE MOBILITY RESEARCH

PART I: INTRODUCTION

Purpose

1. The purpose of this report is to present the results of photoelastic model studies, where gelatin (the photoelastic media) is loaded and penetrated with model probes of nine different configurations, and with a model wheel powered to operate on the gelatin surface under load. Results anticipated from these studies were: the modes of failure of the gelatin media when penetrated by the model probes and the stress distribution therein, the applicability of the gelatin to simulate soil in the model, and the relationship of the stress distribution under the moving wheel load to that developed by the various probes.

Scope

2. Typical photoelastic stress patterns are presented for the model probe loadings and the model of the moving wheel. Both still and moving pictures, in black and white, of the stress pattern have been selected and cover each phase of the study. Also presented are load deformation data for the model probes up to the point of failure. This is correlated with appropriate information from the photoelastic stress patterns. Information is also provided on some of the pertinent physical properties of the gelatin, preparation of the gelatin, testing procedures and pertinent information on the definition and analysis of photoelastic stress patterns. Part II of the report is concerned with the model probe studies; Part III describes the model studies of the moving wheel. Results are discussed, and pertinent conclusions are presented for each study.

Analysis of Photoelastic Stress Patterns

3. Gelatin, glass, bakelite (temporarily), as well as certain other plastics, have the property of becoming doubly refracting when stressed. This property can be seen when a stressed model of such a material is placed between the polarizer and analyzer of a polariscope and viewed through the analyzer. A description of various polariscope arrangements used for photoelastic studies is shown on pages 124-128 of Reference 1. By using a circular polariscope and a monochromatic light source, a fringe pattern such as shown on Figure 1a is obtained. In this case, a nominal 1-inch thick section of gelatin, cast and contained between two glass plates, is loaded on the surface by a rigid 1-inch square plate. The unit load is 1.84 psi. The grid system on the glass side of the container consists of 1-inch squares. The dark fringes are loci of points of equal maximum shear stress, $\frac{p-q}{2}$, where p and q are the major and minor principal stresses. The fringe order, which is marked on the photograph of Figure 1, indicates the relative magnitude of stress for any given fringe. If n is designated as the fringe order, then the maximum shear stress indicated by a fringe is:

$$\frac{p-q}{2} = nF \quad \ldots\ldots\ldots\ldots\ldots \quad (1)$$

where

2F is the fringe calibration value for the model. In this case and for all models discussed in this report, 2F = 0.128 psi.

4. Methods for determining fringe values for model materials are given on page 160 of Reference 1. In the case of gelatin, model fringe values are obtained by adding increments of uniform loading at the surface of the gelatin, as shown on page 345 of Reference 1. Here the maximum shear stress $\frac{p}{\pi}$ has a fringe order of n = 3.5, where p is the unit load applied. (For theoretical correlation of this method of calibration, see pages 68-69 of Reference 2.) Therefore, on Figure 1a, the quantitative values of the maximum shear stress $(\frac{p-q}{2})$ can be obtained at

any point. For example, the maximum fringe count at the lower corner of the loading plate is 13: then using formula (1) with n = 13, and F = 0.064 psi

$$\frac{p-q}{2} = 13 \times 0.064 = 0.83 \text{ psi}$$

Another application is to determine the principal stress at a free or unloaded surface of the gelatin model where the fringe value "n" is about 2.5 at 1 inch from the axis of loading on Figure 1a. Here the principal stress normal to the surface is zero.

Then

$$\frac{p-q}{2} = 2.5 \times .064 \quad \text{or}$$

$$p = 0.32 \text{ psi}$$

Where

p is a tensile stress acting tangent to the surface but within the gelatin.

5. Isoclinics, or lines of equal inclination of the principal stresses, can also be obtained from the stressed model by means of the polariscope. These are obtained by removing the quarter wave plates from the polariscope, and viewing the model through the polarizing plates. If the polarizing elements are crossed at 90° and 0° (the 90° being vertical), one or more dark traces will be observed crossing the isochromatic fringes. This signifies that all along this trace one of the principal stresses, p or q, makes an angle of 90° with the horizontal or x axis of the model. The other isoclinics between 0° and 90° are obtained by revolving the polarizing plates together. Each isoclinic can be traced separately or photographed. The right side of Figure 1b is such a tracing for the stress pattern of Figure 1a. The values of the isoclinics are given in degrees. This angle that the principal stresses make with the x axis is designated as θ_p throughout the report. Determination of the isoclinics provides two other pieces o:

quantitative information about the stress distribution. First, the principal stress trajectories can be drawn as shown on the left of Figure 1b. Secondly, the shear stress τ_{xy} on horizontal and vertical planes (x and y planes) at any point can be computed by means of the relationships indicated for stress at a point shown in Figure 9.

Which is:

$$\tau_{xy} = \frac{p-q}{2} \sin 2\theta_p \quad \ldots\ldots\ldots\ldots \quad (2)$$

Since $\frac{p-q}{2}$ and θ_p are known at any point.

6. Contours of equal values for the shear stress at a point on the x and y planes are shown on Figure 1c in terms of fringes. Formula (2) was used as follows:

$$\tau_{xy} = \frac{n(2F)}{2} \sin 2\theta_p \quad \ldots\ldots\ldots\ldots \quad (2a)$$

Equation (2a) is used to obtain the shear stress in psi for a given contour on Figure 1c by multiplying the fringe value given by 2F, or 0.128 psi.

7. The normal stress distribution on any selected plane in the model can be obtained by means of the shear difference method (see Chapter 8, page 252 of Reference 1). There are other methods of obtaining normal and shear stress distribution on various planes in a photoelastic model; but for the type of photoelastic information developed in this study, the shear difference method is the most applicable.

Construction of Gelatin Models

8. The gelatin in the models was supported in a glass-sided tank 28 3/8 inches long by 10 inches high. The inside clearance between the glass sides of the tank was 1 1/4 inch. The gelatin mass is made by heating granulated gelatin and water in a 15 to 100 parts by weight ratio until a clear solution is attained. This generally requires heating for

one hour in a double boiler arrangement with the water at about 180° F and gelatin at about 170° F. The mixture is then passed through a No. 200 sieve to remove excess air, and siphoned into the glass-sided model mold. A spacer plate is suspended 3/4 inch below the top of the tank. This plate is cut out after set to eliminate surface tension and shrinkage effects at the gelatin surface. The mold sides are removable and are wrapped in aluminum foil prior to pouring. This prevents adhesion of gelatin to the glass and creates a smooth surface on the sides of the gelatin. The model is normally made in the afternoon and tested the following morning. A water layer poured on the surface of the model after the aluminum has been stripped prevents drying of the gelatin and provides a reservoir of lubricant for the glass-to-gelatin contact.

9. The gelatin was formulation-controlled and heated as described above for all models. The temperature during setting and testing was thermostatically controlled, and all models were tested at approximately the same age. Under such conditions, the fringe calibration value (2F) and other physical properties of the gelatin will be reasonably constant from model to model.

10. The fringe calibration value 2F was not measured during the course of tests included in this report. An average value of 2F was used which is based upon 10 calibration tests run on 4 1/2-inch thick models of previous studies using the same gelatin formulation. The fringe value 2F from these tests varied from 0.100 to 0.147. The mean was 0.1275, and the standard deviation was 0.013. The probable deviation is two-thirds of the standard deviation, which indicates that 50% of all calibration values will lie between 0.119 and 0.136. Subsequent to the model testing phase, supplementary calibration tests were run to verify the applicability of the assumed fringe value to the current program. These additional calibrations included line load and semicircular area calibration as well as uniform load calibrations using 1-square inch and 5-square inch rubber bottom containers. The line load calibrations are not well suited to extremely low modulus materials, such as gelatin, because the deflection caused by loading tends to develop an area of contact rather than a line

contact. The mean fringe value 2F using area loadings only was 0.130, which falls within 2% of the mean value reported from the previous studies. It is therefore concluded that the assumed calibration value 2F of 0.128 psi is justified for use because of the exploratory nature of the report. The fringe value is considered adequate for quantitative comparisons of shear and normal stresses.

Physical Properties of the Gelatin

11. Two types of physical tests were made of the gelatin used for the models, direct shear and tensile tests:

a. Direct Shear Tests. These tests were made on cylindrical specimens 2.5 inches in diameter and about 1.5 inches long. The shear load was applied normal to the axis of the specimen, and normal loads were parallel to the axis. A soil type direct shear machine was used. Test results were as follows:

Normal Load, psi	Shear Load at Failure, psi
0	0.71
1.2	1.00
1.4	1.43
1.8	1.22

The above values are plotted on Figure 13, with the normal load as the abscissa and the shear load at failure as the ordinate. A straight line drawn with reference to these points indicates an angle of internal friction ϕ of about 15°, and a cohesive strength of about 0.68 psi.

b. Tensile Tests. Tensile tests were performed on specimens cast in two metal tubes having an inside diameter of 1 3/8 inches. The tubes were placed end to end and taped on the outside. The insides of the tubes were grooved to prevent slippage of the gelatin when the tubes were pulled apart. The test was made with the tubes appropriately gripped

in a vertical position and loaded by adding water to a container attached to the bottom tube. The failure surface was slightly dished. Little or no necking of the gelatin occurred up to failure. Four tests of this type were made. The vertical load at failure divided by the cross sectional area of the gelatin normal to the load gave the following values of tensile strength.

Test Number		Tensile Strength, psi
1		0.95
2		1.03
3		0.93
4		0.88
	Average	0.95

The average tensile strength is shown as a circle on the negative side of the shear versus normal load plot of Figure 13 for the direct shear tests. The circle falls slightly below the extended shear envelope.

PART II: MODEL PROBE TESTS

Test Procedure

General

12. For purposes of description and discussion, the probe models fall into three groups: the rectangular probes, the wedge-shaped probes, and the wheel-shaped probes. In all cases, the probes were 1-inch wide, which was the nominal thickness of the gelatin foundation. Three rectangular probes were tested, and were 1 inch, 2.5 inches and 5 inches in length. All three probes had square end boundaries bearing on the gelatin. In the tests, these sharp corners produced high stress concentration in the gelatin; for this reason, an additional 2.5-inch rectangular probe was studied. This probe had the end contact corners rounded to an 0.125-inch radius. The second group of probes consisted of symmetrical wedges having vertex angles of 30°, 45°, and 90°. The wheel-shaped probes were 3 inches in diameter. For one of these probes, the semicircular surface was flat in the wide dimension; the other two probes had a toroidal shape in this dimension.

Loading

13. The probes were loaded by adding lead shot to a sheet metal box attached directly to the probe. The box was 5 inches high, and conformed to the depth and width of the probe. Under each increment of load up to failure of the gelatin foundation, the deflection and the maximum fringe value were recorded. The bearing area of the probe is the surface in contact with the gelatin, and is scaled from photographs taken at the time a given load increment is applied. The stress pattern in the gelatin was photographed at selected periods. The isoclinics were traced for selected loadings. In order to get reasonably complete information, several gelatin foundation models were cast for each of the probe tests. After initial failure of the gelatin occurred, the load acting could not be measured by the above methods; since the load would immediately decrease, and then build up as resistance to further penetration developed.

An attempt was made to load the probes by means of an air piston in order to obtain load measurements after failure of the gelatin; this was unsuccessful insofar as measurement of load was concerned. Moving pictures were taken of the stress patterns in order to obtain a concept of stress development while the probes penetrated the gelatin foundation. The motion pictures also show the isoclinics for the 90° wedge-shaped probe in a static position. Table A lists these movies in their sequence on the film accompanying this report.

Table A

Moving Picture Record of Stress Pattern Development by Penetration of Model Probes into Gelatin

Type of Model Probe	Method of Loading	Average Rate of Penetration, in./sec.***	Total Time of Loading, Seconds
1-inch Flat Plate	Loading Frame*	0.10	59
5-inch Flat Plate	Loading Frame	0.07	62
2 1/2-inch Rounded	Air Piston	0.15	14
30° Probe	Air Piston	0.15	41
30° Probe**	3/8" rod by hand	0.10	32
45° Probe	Air Piston	0.20	12
45° Probe**	3/8" rod by hand	0.20	21
90° Probe	Air Piston	0.20	61
Semicircular	Air Piston	0.07	41

* Yoke driven by a screw jack.

** Metal casing making probe continuous at top removed. Figures 6b and 6c show this difference.

*** Values obtained from film by counting frames.

14. The inconsistency in the rate of penetration for the various probes listed in Table A is due to experimenting with methods of

measuring the magnitude of the load with reference to penetration. Under these conditions, the rate of penetration is influenced by the shape of the probe as well as the method of load application. Up to the point of initial failure, the stress patterns on the motion picture film compare well with the patterns obtained by static loading with lead shot. The rate of penetration does not influence the character of the failure in the gelatin; but it is likely that it would influence the relationship of the rate of penetration versus load after initial failure, by increasing the rate of tearing. A plot of load versus time would indicate an increase in resistance to penetration as the probes penetrate the gelatin. A peak load would be obtained at the instant of failure. Certain probes (such as the 2 1/2-inch rounded plate, the 45° probe, the 90° probe, and the semicircular probe) develop a sudden rapid increase in rate of penetration immediately after initial failure. The increase of penetration for other probes advances at a reasonably constant rate before and after failure. In all cases, a marked rearrangement of fringes occurs, and the influence of side friction or plate resistance is clearly indicated. The magnitude of stresses observed after failure appears to be a function of how the fringes redistribute after failure. This new pattern is, in turn, affected by how rapidly the cracks in the gelatin develop; and is strongly influenced by the rate of penetration immediately after failure.

Test Results

15. Table 1 summarizes and reduces the information obtained from the loading of the model probes. Generally, data for two loadings on each probe are given; one prior to failure of the gelatin foundation, and one just at failure. The bearing area for the wedge-shaped probes, the semicircular probe, and the toroidal semicircular probe is taken as the area in actual contact with the gelatin foundation for a given load; and is used as the basis for computing the unit load. The maximum shear stress "τ_{max}" given in Table 1 is that for the maximum fringe order "n"

observed for the given loading. It is computed as follows:

$$\tau_{max} = nF$$

where

$$F = 0.064 \text{ psi}$$

16. More detailed information on the load, deflection, and stress measurements for the rectangular and semicircular probe models is given on Figures 10-12. Figure 10 shows load versus maximum fringe value; Figures 11 and 12 are plots of deflection against load and maximum fringe values. All values plotted in these figures are given in Table 2. The toroidal-shaped semicircular probe performed the same as the semicircular probe with the flat transverse surface. The 45° wedge-shaped probe caused failure of the gelatin under such low loads that no static loading data were obtained. In the case of the 30° and 90° wedge-shaped probes, only data for the static condition at failure were obtained for the same reason.

17. Figures 1-4 show the isochromatic fringe pattern for a selected loading of each of the rectangular model probes. The loading for each probe is the same as the loading prior to failure, and given in Table 1. Figure 1b gives the isoclinic pattern corresponding to the fringe pattern of Figure 1a. Only half the isoclinic pattern is shown, since it is symmetrical about the axis of the loaded area. On the left half of Figure 1b, the trajectories of principal stress derived from the isoclinic pattern are shown. This isostatic pattern is also symmetrical about the axis of the loaded area. Figure 1c shows contours of the computed values of τ_{xy}, the shear stress at a point on the vertical and horizontal planes of the model foundation. The shear stress at a point is always equal on planes at 90° to each other. A similar development is shown for Figures 2-4.

18. Figures 6b and 6c show the isoclinic pattern for the 45° wedge-shaped probe at appreciable penetrations into the gelatin foundation, after initial failure. These figures differ in that the sheet metal form

conforming to the top of the probe was used with 6b while it was omitted for 6c. There are no Figures 6a or 6d.

19. Figures 5a and 7a show the isochromatic patterns for the 30° and 90° wedge-shaped probes, just as initial failure is occurring beneath the point of the wedge. The isoclinic pattern, principal stress trajectories, and τ_{xy} contours for the stress pattern are also shown with Figures 5 and 7. Figures 5d and 7d show the isoclinic pattern after initial failure, when the 30° and 90° wedges have penetrated an appreciable depth into the gelatin foundation.

20. The isochromatic pattern for the semicircular probe at a load of about one third the failure load is given on Figure 8a; additional information and development is shown on Figures 8b and 8c.

21. One of the important results is the mode of failure when the loading of the various probes exceeded the strength of the gelatin foundation. In the case of the four rectangular probes, initial failure occurred as a horizontal parting of the gelatin. This parting, or tearing of the gelatin, started at the corner of the probe in contact with the gelatin surface in the area of high stress concentration, after the gelatin had deformed anywhere from 1 to 2 inches. In the case of the wedge-shaped probes, initial failure occurred as a vertical split originating at the point of the wedge. For the 30° probe, the deflection of the gelatin at failure was 1-inch; and for the 90° probe, 0.6 inch. The initial failure of the gelatin foundations under the loading of the semicircular probes occurred as a vertical split in the gelatin foundation along the axis of the loaded area. The split originated directly beneath the probe, in an area of high stress concentration, at a deflection of 2.9 inches.

22. The initial failures described above are shown on the moving picture film strip accompanying this report. In some cases, as the loading or movement of the probe into the gelatin foundation progressed, a secondary type of failure developed along with additional splitting. This secondary type of failure consisted of a remolding of the gelatin beneath the probe, and was particularly evident in the case of the rectangular probes.

Discussion of Results

General

23. From a dimensional standpoint, the model simulation to a vehicle wheel on soil for the probe loadings is only approximate, since the model represents a condition of two-dimensional strain. Thus, the stress conditions shown for the probes would most closely represent strip-loadings of infinite length. Secondly, the gelatin has different strength and deformation characteristics than a weak soil. Gelatin has appreciable tensile strength, and deforms elastically to about initial failure under the loading of the probes. The chief advantage of gelatin is that stress patterns can be obtained at large deformations prior to failure, and after failure, under predetermined types of loading. This is the chief reason that it was selected for these exploratory studies.

Deflection and Maximum Shear Stress

24. The deflections with regard to load and maximum fringe values are well summarized on Figures 10-12 for the rectangular and semicircular model probes. The last point plotted on each curve of the above figures is the deflection for the load at failure; there is no sharp break up to this point for any of the curves, except on the load versus deflection curves (Figure 11) and load versus maximum fringe order (Figure 10) for the semicircular probe. This occurs, in this instance, because unit loads are plotted, and the area taken for the semicircular probe is the area in contact with the gelatin. Therefore, the area used in computing the unit load increases as the deflection increases. This influence is not present in Figure 12, where the deflection is plotted against the maximum fringe order. Here, the curves for the various probes make fairly straight lines. This would indicate that the gelatin showed a reasonable amount of elasticity up to the point of initial failure under the rate and magnitude of loadings applied. It should be pointed out that the gelatin will deform slowly under a given load increment; hence, the deflection reading is quite dependent on the time a given increment of load has been acting. Varying amounts of time were spent in applying the initial load

increments, as well as subsequent ones for the various probes. This would account, to some extent, for deviations in the curves of Figures 10-12 from a straight line. In any event, it can be concluded that the gelatin exhibited a greater tendency toward elastic behavior than a weak soil would at similar deformations.

25. If the unit load at initial failure is divided by the corresponding deflection for the rectangular shaped probes, a so-called modulus of subgrade reaction can be obtained for purposes of comparison. This reduction is shown in the following Table B:

Table B

Subgrade Modulus - Rectangular Probes

Type of Model Probe	Unit Load at Failure, psi	Deflection, inches	Subgrade Modulus, lbs./in.^{3}
1-inch Flat Plate	2.75	0.95	2.90
2 1/2-inch Flat Plate	2.40	1.60	1.50
2 1/2-inch Rounded	3.64*	2.30	1.58
5-inch Flat Plate	2.16	2.00	1.08

* Contact Area = 2.5 in.^{2}

As would be expected, the subgrade modulus decreases as the loaded area increases. Moduli of the order shown in the above table would be representative of a very weak soil. The effect of rounding the corners on the 2.5-inch probe is quite evident in terms of initial failure load and corresponding deflection; however, this modulus is not too different from the 2 1/2-inch plate with the unrounded corners.

26. The deflection of the wedge-shaped probes at initial failure is quite small and difficult to measure with respect to load. No load deflection measurements were obtained for the 45° wedge. Such measurements were obtained only for the 30° and 90° wedges. As may be seen from Table 1, failure of the 90° wedge occurred at slightly over twice the total load

causing failure for the 30° wedge; the deflection was slightly less at failure for the 90° wedge. If further tests are made on wedge loadings for gelatin models, a more elaborate loading device will be necessary.

27. An interesting method of comparing the behavior of the rectangular and circular probes is to compute concentration factors, K, on the basis of the maximum shear stress measured at various loadings. The concentration factor for a given unit load "p" on a probe is taken as the maximum shear stress produced for load "p" divided by the quantity $\frac{p}{\pi}$, where $\frac{p}{\pi}$ is the maximum shear stress for a uniform load on an elastic foundation of semi-infinite extent in two dimensions. This computation for the rectangular and circular probes is shown in the following Table C. The load "p" and corresponding deflections are taken from Table 2. The maximum shear stress is obtained by multiplying the appropriate fringe value in Table 2 by the model fringe value, 0.064 psi/1 fringe.

Table C

Summary of Concentration Factors for Rectangular and Circular Probes

Type of Model Probe	Measured			Concentration Factor*
	Load, psi	τ_{max}, psi	Defl., in.	
1-inch Flat Plate	1.40	0.77	0.70	1.72
	1.84	0.83	0.80	1.42
	2.75**	1.02	0.95	1.17
2 1/2-inch Flat Plate	0.99	0.77	0.80	2.44
	1.95	1.02	1.30	1.65
	2.40**	1.15	1.60	1.51
5-inch Flat Plate	0.80	0.83	0.90	3.26
	1.94	1.34	1.80	2.17
	2.16**	1.41	2.00	2.05
2 1/2-inch Plate, Rounded (See Note)	0.80	0.45	0.90	1.77
	1.64	0.77	1.40	1.48
	3.19**	1.09	2.30	1.07
3-inch Semicircular (See Note)	1.03	0.45	0.90	1.37
	1.84	0.77	1.65	1.32
	2.86**	1.28	2.90	1.41

* Concentration Factor, $K, = \frac{\tau_{max}}{\frac{p}{\pi}}$

** Load at Initial Failure

Note: Surface area used for computations is the actual contact surface rather than a projected area.

Probably the best concentration factors to compare are those obtained for the lower loads. The lower the concentration factor, the more nearly the probe loading approaches the performance of a uniform load. For the lower loadings, the order in which the various probes approach the effect of uniform loading would be as follows: (1) circular probe, (2) 1-inch plate, (3) 2 1/2-inch plate, rounded, (4) 2 1/2-inch flat plate, and (5) 5-inch flat plate. At the failure load, the 2 1/2-inch rounded plate more nearly approaches the condition of uniform loading than the 1-inch flat plate. The 2 1/2-inch plate with the rounded corners also appears to more nearly approach the condition of uniform loading at failure than does the circular probe. If the contact area for the 2 1/2-inch plate with rounded corners is taken as 2.5 square inches, instead of the surface area in contact with the gelatin, the concentration factors for this plate become 1.56, 1.28, and 0.94 as compared to 1.77, 1.48, and 1.07 shown in Table C. Table C also shows that as the load on the probe increases, the concentration factor is reduced. This reduction is greatest for the rectangular probes, and least for the semicircular probe. It is interesting to compute the concentration factors for the circular probe, assuming that the contact area for the various loads is the plan projection of the surface in contact with the gelatin rather than the area of the surface in contact with the gelatin assumed for the tabulation. This results in concentration factors 1.25, 1.07, and 0.97 as compared to 1.37, 1.32, and 1.41 given in Table C for the circular probe. The chief conclusion that can be drawn from the above discussion is that the semicircular probe produces the least distortion of stress development as it is loaded to initial failure, since the variation in concentration factors is less.

Stress Patterns

28. General. The stress patterns shown for the various probes on Figures 1-5 and Figures 7 and 8, prior to failure of the gelatin foundation, are essentially what one could infer from the theory of elasticity and photoelastic studies of similar nature. Basically, where a stress pattern is produced either prior to or after initial failure, it is characteristic of that in an elastic media. The actual pattern is influenced

by the boundary conditions which are the shape of the loading probe, the depth and length of the gelatin in the tank, boundary changes at the surface due to large deformations of the gelatin, and discontinuities created in the gelatin mass due to local failure.

29. Rectangular Probes. In all cases for the rectangular probes, the normal stress distribution beneath the probes prior to initial failure is quite high at the boundaries and falls to about a half to one third of this value toward the axis of the load. This is exactly the opposite of the distribution one would expect beneath a loaded rigid plate on a weak cohesive soil, where the greatest normal stress would be expected to occur beneath the center of the plate. This effect is minimized, however, after initial failure has occurred and the gelatin beneath the plate has been remolded by confining stresses under the plate. It would be interesting to study this further by means of a load-deflection curve for the full range of penetration shown by the movie strip, and with a companion curve for a weak cohesive soil loaded with a rectangular probe. The 2 1/2-inch rectangular probe with the rounded edges will come closer than the rectangular probe with square corners to producing stress conditions in the gelatin that one would expect to occur when a weak cohesive soil is loaded by means of a rectangular plate. The stress pattern for the 5-inch rectangular plate is well defined in the vicinity of the plate; however, the deflections and failure of the gelatin beneath this plate were likely influenced by the lower rigid boundary of the gelatin, since it is only twice the length of the plate below the surface of the gelatin. There is a high concentration of shear stress at the corners of the rectangular plates which falls off rapidly toward the center of the plates. It is in this area of high shear stress that initial failure occurred. Failure occurred here probably because there is a complete reversal of shear stress on the vertical plane where it intersects the 90° isoclinic.

30. Wedge-shaped Probes. When the wedges first contact the gelatin they produce a line load. In this case, the isochromatic pattern developed is a series of circles all tangent at the point of application of the line load (see page 42 of Reference 2). This pattern is still dominant on Figures 5 and 7, even though part of the wedge loading is being

transmitted to the gelatin by the sides of the wedges. In both instances, the maximum fringe order is produced by a normal reaction along the sides of the wedge and away from the point of the wedge. It is possible that failure of the gelatin has already occurred at the point of the wedge and the concentration of stress relieved there. The normal and shear stress distribution along the sides of the 30° and 90° wedges that would result from the patterns on Figures 5 and 7 may be fairly close to what one would expect for a weak cohesive soil. The 90° isoclinics indicate a reversal of shear stress at the point of the wedge and where the side of the wedge leaves off contact with the gelatin surface.

31. Semicircular Probes. Since the patterns for the flat semicircular probe and the toroidal shaped probe were similar, only the stress patterns for the semicircular probe with the flat transverse surface will be discussed. The configuration of the isochromatic fringe pattern on Figure 8 resembles that for uniform loading on a semi-infinite plate (see page 67 of Reference 2). The normal stress distribution is likely to be reasonably near that experienced by a weak cohesive soil loaded by a flat rectangular plate. The mode of failure of the gelatin under the circular probe is interesting. On Figure 8, the maximum fringe order n is 8. This occurs directly under the loaded area and about 0.5 inches below the load contact surface. When initial failure occurred, a vertical split took place when the fringe value reached 20 at this point. Failure was progressive with the initial split extending to the loaded surface and down into the gelatin. Initial failure took place at the point of maximum shear stress. This is shown on the motion picture film.

32. Strength of Gelatin Versus Stress Conditions Beneath Probe Loadings at Failure. This comparison, at first glance, would appear to be relatively simple since all failures of the probes took place at the point of maximum shear stress; and for the rectangular and circular probes, the maximum shear stress averaged 1.19 psi with a maximum of 1.41 psi and a minimum of 1.02 psi. In paragraph 11, results of tensile strength tests and direct shear tests are given for the gelatin. An average tensile strength of 0.95 psi is given. If it is assumed that the gelatin has an angle of internal friction of zero, then its maximum shear strength would

be one half the tensile strength, or about 0.5 psi. This is less than half the maximum shear stress observed in the gelatin at initial failure under the probe loadings. While the direct shear test results given in paragraph 11 and Figure 13 are not too conclusive, they do indicate that the gelatin may have an angle of internal friction. This then would mean that the strength of the gelatin at failure is dependent on the combination of principal stresses acting at the point of failure. A further complication arises since the stress in the gelatin beneath the probes is three-dimensional because of the confining glass plates. Only the strain is two-dimensional. However, if we assume that the gelatin has the angle of internal friction and cohesion shown on Figure 13, and that the stress in the gelatin under the loading of the probes is two-dimensional, the principal stresses at the point of failure can be obtained since the maximum shear stress at the point of failure is known. Therefore, all that is necessary is to use the maximum shear stress as a radius and draw the Mohr circle tangent to the shear envelope for the gelatin. This can also be done analytically. The following Table D gives the unit loading of the probe at initial failure, the maximum shear stress for the failure load, and the derived major and minor principal stresses.

Table D

Principal Stresses at Point of Failure
for Rectangular and Circular Probes

Type of Model Probe	Load at, Failure, psi	τ_{max}, psi	Principal Stresses, psi	
			Major	Minor
Semicircular	4.15*	1.28	-1.00	-3.56
2 1/2-inch Flat Plate, Rounded	3.64*	1.09	-0.50	-2.68
1-inch Flat Plate	2.75	1.02	-0.30	-2.34
2 1/2-inch Flat Plate	2.41	1.15	-0.64	-2.94
5-inch Flat Plate	2.16	1.41	-1.30	-4.12
(-) Compression				
* The failure load is computed on the basis of the projected area.				

The use of τ_{max} in the derivation is permissible because in all cases initial failure originated at the precise location of the observed maximum fringe value. It will be noted that the probes listed in Table D are arranged in the order of increasing stress concentration factors at failure as shown in Table C, paragraph 27. The principal stresses are all compressive stresses. In the case of the semicircular probe, the minor principal stress is about 0.86 of the unit load acting. For uniform loading on a semi-infinite plate, the theory of elasticity gives a ratio of 0.80 p for the vertical or minor principal stress at the point of maximum shear stresses. It also indicates a ratio of 3.0 between the minor and major principal stresses at the location of the maximum shear stress as compared to 3.6 in the table. When the principal stresses for the other probes are examined with respect to the stress trajectories, mode of failure, and location of the failure point, they do not appear unreasonable. For example, in the case of the 2 1/2-inch and 5-inch plates, failure occurred at the corner where the normal load acting was undoubtedly greater than the applied unit load. In these two instances, the minor principal stress is greater than the unit loading. These two probes also had the highest concentration factors. A similar examination can be made for the 30° and 90° wedge-shaped probes. However, referring to Figures 5 and 6, it has been indicated previously that the maximum fringe order does not correspond to the point of initial failure which took place at the point of the wedge. On Figures 5 and 6 the maximum fringe order is 8 for the 30° wedge, and 9 for the 90° wedge at the point of failure. These fringe orders may have been higher before the gelatin split. The following Table E gives the maximum fringe order, the maximum shear stress for the failure load, and the derived major and minor principal stresses.

Table E

Principal Stress at Point
of Failure for Wedge-Shaped Probes

Type of Model Probe	Max. Fringe Order	τ_{max}, psi	Principal Stresses, psi	
			Major	Minor
30° Wedge	8	0.512	+1.040	+0.016
90° Wedge	9	0.586	+0.800	-0.372
(+) Tension (-) Compression				

The above analysis of the possible failure conditions beneath the probes is presented for qualitative comparisons and for ideas that may be used if further more precise studies of this type are made. In conclusion, it appears that the initial failure at a point in the gelatin mass may be similar under the probes at failure to what occurs in a weak cohesive soil. However, the progression of failure after failure at a point in the gelatin occurs bears no resemblance to what occurs in a weak cohesive soil mass.

Summary and Conclusions

33. Under the loading by the various probes, the gelatin exhibited elastic behavior to a greater degree with regard to deformation and stress increase up to initial failure than would a weak cohesive soil subjected to deformations of the same magnitude.

34. The semicircular probe and the 2 1/2-inch flat plate with rounded corners produced less distortion in the build up of maximum shear stress to the point of initial failure than did the 1-inch, 2 1/2-inch, and 5-inch plates.

35. The stress distribution at the contact surface of the rectangular plate probes at loadings less than their initial failure load on gelatin is quite different than that for a rigid plate loading on a weak cohesive soil.

36. The stress distribution along the contact surface of the semicircular probe on a gelatin foundation is similar to that expected for a rigid rectangular plate loading on a weak cohesive soil.

37. The stress distribution along the contact surface of the wedge-shaped probes before initial failure of the gelatin appears to be reasonably compatible with what might be expected when this type of probe penetrates a weak cohesive soil.

38. The rupture surfaces observed in the gelatin for the various probes after initial failure had occurred at a point are not compatible with failure surfaces that would take place in a weak cohesive soil under similar loading.

39. With the possible exception of the wedge-shaped probes, initial failure in the gelatin took place at the point of maximum shear stress. This may or may not be true for a soil under similar conditions of loading.

40. Sufficiently conclusive information was not developed during these studies to correlate the strength of the gelatin with stress conditions at failure under the loading of the model probes tested. However, this aspect of the study is discussed in paragraph 32 and a possible approach indicated.

41. These studies have been exploratory; and as a result, the information developed is incomplete in some respects. However, the results and experience obtained do indicate quite clearly what is pertinent if further studies of this type are made. The following should be considered:

a. Development of detailed information on the physical properties and strength characteristics of the photoelastic materials used.

b. Adequate instrumentation and improved techniques should be planned well in advance of actual model testing.

c. Further investigations should be concerned with the semicircular and wedge-shaped probes or shapes other than the rectangular plates.

PART III: MOVING WHEEL LOAD STUDIES

Test Procedure

General

42. Five gelatin foundation models were constructed as described in paragraph 8. Penetration tests were made on each foundation model up to 1-inch deflection with the 3-inch diameter semicircular probe. The relationships between load, deflection, and fringe value were similar for each model foundation as well as for the foundation models tested with the semicircular probe described in Part II. These relationships for the semicircular probe of deflection, load, and maximum fringe value are plotted on Figures 21-23. The difference between these curves and those shown on Figures 10-12 for the semicircular probe is that total load rather than unit load is plotted; and they are better defined in the range of 0 to 1-inch deflection. The moving wheel load tests of the five foundation models are developmental in character. The developmental aspects are: the method of applying the moving wheel load, control of speed and slip of the wheel on the gelatin surface, and photographic techniques for recording isochromatic and isoclinic patterns. This development is best indicated by the following description of the five model tests.

a. Model No. 1 - Towed Wheel. An aluminum wheel was pulled across the gelatin surface with negligible friction developed between wheel contact and the gelatin. Four runs were made and the isochromatic patterns recorded on moving picture film.

b. Model No. 2. The wheel was fitted with a cog belt to produce some friction between the wheel and gelatin contact surface. Nine runs were made. Slip of the wheel was controlled; however, speed was not controlled. A moving picture record of the isochromatic patterns for each run was made. Slip as used in this report is positive, and is defined as one minus the ratio of the actual wheel advance per revolution to the circumference of the wheel. Thus, if the distance the wheel advances in one revolution is equal to its circumference, the slip is zero.

c. Model No. 3. Some friction was obtained between the wheel contact and gelatin surface by using a grit belt on the wheel. Nine runs were made with this model. Both speed and slip of the wheel were controlled. Five runs were made at 0 slip, and four runs were made at +25% slip. Moving pictures were made of the isochromatic patterns for each run.

d. Model No. 4. Wheel loading and procedures were the same as for the preceding Model No. 3. Moving pictures were made of the isoclinic development at 0 slip, +25% slip, and +50% slip.

e. Model No. 5. This model was similar to the preceding Model Nos. 3 and 4. For this model, flash pictures were taken of the isochromatic stress pattern with a still camera. This provided a better defined isochromatic pattern than the moving pictures. A picture was taken of the isochromatic stress pattern at 0 slip, +25% slip, +50% slip, and also for the semicircular probe. This probe produced the same deflection and stress pattern as the moving wheel in a static position.

Wheel Loading

43. The 3-inch diameter by 1-inch wide aluminum wheel apparatus used to load the gelatin foundations was furnished by the WES, and is shown suspended in the glass sided tank in Figure 14a. The wheel in contact with the gelatin was driven initially by turning the wheel in the carriage with a crank; however, the aluminum wheel would not develop sufficient friction with the gelatin to move the assembly across the surface. Therefore, in the tests of Model No. 1, the assembly was towed and the wheel in contact with the gelatin did not revolve. In order to continue with the moving wheel load tests, it was necessary to modify the loading apparatus so that the wheel would turn and develop frictional contact with the gelatin.

44. The apparatus shown in Figure 14a provides positive linkage between the driven and load wheels through a belt drive. The axle for the wheel is mounted rigidly to a carriage that runs on the track located above the tank (see Figure 14b). The load wheel is linked to a wheel of the same diameter mounted on a parallel axle in the carriage. An 0.25-inch wide timing belt provided the linkage between the wheels. This belt

is set flush with the surface of the two wheels and centrally aligned. (Note that on Figure 14b, the gear belt is covered by the grit belt used for Models 3, 4, and 5.)

45. The elevation of the track is adjustable to permit controlled deflection of the gelatin. Loading of the gelatin surface is accomplished by lowering the tracks and the carriage so that the lower wheel produces a predetermined deflection and fringe pattern in the gelatin at the static position. Since the wheel has the same diameter as the semicircular probe, the approximate total load on the gelatin can be determined in grams from the graphs of either Figure 21 or 22.

46. Positive slip control comes about through the linkage provided by various gear wheels in contact with the gear rack. The gear wheel attached to the carriage (Figure 14b) is 3 inches in diameter, and when turned with a crank will advance the load wheel at a constant rate with 0 slip. The gear wheels of lesser diameter lying on the bed of the carriage are used with the carriage and rack to advance the load wheel at +25% and +50% slip.

47. To obtain frictional resistance in the tests of Model No. 2, a 3/4-inch wide timing belt was used with the protuberances or cogs turned outward so that they would be in contact with the gelatin. The cogs on the timing belt protruded about 0.125 inches from the belt surface. As will be seen from the results, reasonable consistent stress patterns were obtained in the gelatin for the nine runs made with the cog belt. There are two disadvantages to this arrangement. First, a high concentration of stress occurred where the cogs came in contact with the gelatin surface; and second, propelling the carriage and load wheel with the crank was jerky and produced some distortions in the stress pattern.

48. The areas of high fringe order show what may occur between deep tire treads, but do not simulate the effect of a smooth wheel on an elastic medium. This effect can be more nearly simulated by replacing the cog belt with a belt having less pronounced protuberances. The belt material selected was an open weave emory cloth without backing. This cloth, when cemented together and tightly fitted to the assembly wheels, forms the grit belt used for Model Nos. 3, 4, and 5 (Figure 14b).

49. The final step in the design evolution was to reduce the jerky motion due to hand crank activation. A fractional horsepower motor with a speed reducer was installed to drive the carriage. This then permitted the rate of advance of the carriage to be controlled by a current regulator on the circuit to the motor. The motor mounted on the carriage is shown on Figure 14.

Wheel Slip Control

50. Slip as defined in paragraph 42b is one minus the ratio of the actual wheel advance per revolution to the circumference of the wheel. This is shown graphically on the trace photographs of Figure 15. These photographs were obtained by mounting a small light source on the rim of the wheel and a second light source on the frame. The traces of the two light sources were photographed by opening the camera shutter and driving the wheel across a focused area in a darkened room. Figure 15a shows the trace for the moving wheel geared for 0 slip; Figures 15b and 15c show the cycloids for +25% and +50% slip respectively.

Photographic Techniques

51. There were three photographic techniques used for recording the isoclinic and isochromatic patterns produced by the moving wheel load. The moving pictures of the isochromatic stress patterns were obtained using a white light source in a circularly polarized polariscope, and a monochromatic filter mounted on a 16 mm motion picture camera. The camera speed was 16 frames per second. This photographic procedure was used for Model Nos. 1, 2, and 3. The photographic procedure for Model No. 4 is the same as above except that a crossed plane polariscope was used to emphasize the isoclinics, and the monochromatic filter was removed from the camera. The photographs of Figures 17(a), 18(a), and 19(a), show the isochromatic stress patterns for the moving wheel load at 0, +25%, and +50% slip for Model No. 5. These photographs were obtained with a still camera fitted with a monochromatic filter. The light source in the polariscope was replaced with a standard electronic flash. The stress pattern in the gelatin was photographed by flashing the light at a given instant with the camera shutter open. This effectively stopped the motion of the

moving wheel and recorded the instantaneous fringe pattern in the gelatin.

Measurements

52. In addition to information obtained from the isochromatic and isoclinic patterns, three other types of information were obtained, they are:

a. Deflections. All deflections measured are the maximum deflections of the gelatin under the wheel loading. This is the difference between the original surface elevation of the gelatin and the elevation of the gelatin directly beneath the load wheel. These measurements were obtained from the moving picture film and from photographs taken of the moving wheel load.

b. Forward Speed of the Moving Wheel. This was obtained by counting the number of frames for a given run and dividing this value by the film speed (16 frames/sec.). This procedure was checked by timing the runs with a stop watch.

c. Gelatin Differential. Again, this measurement was obtained from the moving picture and photographs. It is the difference in elevation of the gelatin surface about 0.5 inches fore and aft of the moving wheel.

d. Contact Area. This measurement was obtained from the moving pictures and photographs by scaling the chord length of the portion of the wheel or semicircular probe in contact with the gelatin surface. The wheel contact area was then computed using the chord length, radius, and width of the wheel.

Test Results and Discussions

General

53. The basic results of the five models tested are given by the moving picture film accompanying this report, and by the photographs of Figures 16(a), 17(a), 18(a), and 19(a). The initial sequence of the moving picture film describes the apparatus used to apply the moving wheel load. This is followed by isochromatic patterns for Model Nos. 1, 2, and

3, and finally the isoclinic development for Model No. 4 at 0, +25%, and +50% slip. The basic isochromatic stress patterns for Model No. 5 are given by the photographs of Figures 17(a), 18(a), and 19(a) at 0, +25%, and +50% slip. The following paragraphs present the results with a brief discussion in the order of the model test sequence.

Model No. 1

54. Test Results. The information contained in the following Table F was taken from the moving picture film accompanying this report.

Table F

Measurements from Model No. 1 - Towed Wheel

Run No.	Defl., in.	Max. Fringe Order	Forward Speed of Wheel, in./sec.	Gelatin Differential, in.
1	0.38	3 to 2	1.0	0.25
2	0.38	4 to 3	1.0	0.25
3	0.38	4 to 3	2.3	0.25
4	0.88	5 to 4	0.8	0.25

For all four runs, the configuration of the fringe pattern was similar. In all cases, the fringe value at the start of a run was higher than at the end. There was a measurable change in deflection as the wheel advanced over the surface. This slight change was enough to account for the change in fringe order. No friction between the wheel and gelatin was available, and the towed wheel did not revolve as it was pulled across the gelatin surface at either a deflection of 0.38 or 0.88 inches.

55. Discussion. The forward speed of the wheel did not affect the maximum fringe value. This is shown in Table F, where the speed for Run No. 3 was over twice that for Run No. 2 at the same deflection. Referring to Figure 23, which gives the maximum fringe order-deflection relationship for the semicircular probe, the maximum fringe value for a

deflection of 0.38 inches is about 3, and for a deflection of 0.88 inches the value is about 7. Table F indicates a fringe order of 3 and 5 respectively for these deflections. This would tend to indicate an equivalent or lower stress for the moving wheel load than for the static loading. This is inconsistent with the results obtained for the other moving wheel load studies, where friction between the gelatin and wheel was present. For this condition, the maximum fringe value is generally greater than for the static case. There is some indication from the moving picture that the gelatin adhered to the glass sides of the tank; therefore, any conclusions concerning the maximum fringe values for the towed wheel are questionable. To clarify the matter these model tests should be rerun.

Model No. 2

56. Test Results. This is the model run with the cog belt. The following Table G summarizes the results from the moving picture sequence for this model.

Table G

Model No. 2 Measurements - Moving Wheel Cog Belt

Run No.	Defl., in.	Max. Fringe Order (Dominant Pattern)	Forward Speed of Wheel, in./sec.	Slip in %	Gelatin Differential, in.
1	0.9	9.0	2.3	0	0.25
2	0.9	9.0	2.5	0	0.25
3	0.9	9.0	1.3	0	0.25
4	0.9	8.0	1.2	+50	0.13
5	0.9	9.0	2.5	+50	0.13
6	0.9	8.0	1.6	+50	0.13
7	0.9	7.0	Static Load		--
8	1.2	9.0	0.9	+50	0.38
9	1.5	12.0	0.6	+50	Failure

The moving picture of the runs listed in Table G indicates that the dominant stress pattern is quite similar to that of the smooth wheel.

However, at the points where the cogs contact the gelatin surface, there are local stress concentrations. The maximum fringe value given in the third column of Table G is from the dominant stress pattern, and occurs in the gelatin foundation a short distance below the wheel as with the circular probe. During Run No. 8, failure started about midway on the gelatin surface beneath one of the cogs. Complete failure of the gelatin foundation took place during Run No. 9, and progressed from this initial failure.

57. Discussion. A static loading to 0.9 inches deflection was placed on the gelatin with the cog wheel for Run No. 7. The maximum fringe value, neglecting the stress concentration at the cogs, was 7.0. This same maximum fringe value is indicated for the circular probe on Figure 23 at 0.9 inches deflection. However, for the moving wheel at this deflection, the maximum fringe value was greater as may be seen from Run Nos. 1 through 6 on Table G. Therefore, it can be tentatively concluded that a moving wheel load produces greater stress in the foundation than an equivalent static loading. With the exception of Run No. 5, there is an indication that the maximum fringe value is greater for 0 slip than for +50% slip. It follows that the stress is greater for 0 slip than for +50% slip. At 0 slip, the gelatin differential ahead of the wheel is greater than for +50% slip for runs at the same deflection (see Table G). For Run No. 8, the deflection was increased from 0.9 inches to 1.2 inches. Referring to Figure 22, this would indicate that the load on the moving wheel was increased from about 1050 grams to approximately 1700 grams. At this latter loading, initial failure occurred in the gelatin surface. For Run No. 9, when the deflection was increased to 1.5 inches or an approximate load of 2300 grams, complete failure of the gelatin foundation took place. In the case of the static loading for the semicircular probe, initial failure in the gelatin foundation occurred at a deflection of 2.9 inches and a load of 5600 grams. The failure under the moving wheel load was undoubtedly accelerated by the tearing action of the cogs which occurred as repetitive runs were made across the gelatin surface. Some minor marring of the surface became evident by the third run. As the wheel advanced across the gelatin for the eighth run, a small tension

crack appeared slightly to the right of the center vertical grid. This developed initially when the center of the advancing wheel was still about 2 1/2 inches away. After completion of the eighth run, the crack moved about 3/4-inch into the gelatin. After the ninth run, this crack extended to the final failure state. It is probable that initial failure at 1.2-inch deflection progressed from one of the minor blemishes noted during the third run. Table H below presents a comparison of the initial failure conditions for the moving wheel with those of the semicircular probe and 1-inch flat plate given in Table 1 at the end of this report.

Table H

Comparison of Load and Stress Conditions at Initial Failure for Probes and Moving Wheel Load

Load Condition	Load, gms	Defl., in.	Max. Fringe Order
Moving Wheel - Cog Belt	1700	1.20	12
Semicircular Probe	5600	2.90	20
1-inch Flat Plate	1250	0.95	16

It is obvious from Table H that the failure conditions for the semicircular probe are not close to the conditions of initial failure for the moving wheel with the cog belt, even though there is considerable similarity between the dominant isochromatic patterns. The 1-inch flat plate probe more nearly simulated load, deflection, and stress conditions at initial failure for the moving wheel. Final failure appeared on the ninth run when one of the cogs moved under the vertical axis and was directly over the area of maximum shear stress. The approximate order of fringe build up at the cog was 4; while the build up to the point of maximum shear stress was 12. If it is assumed that these are additive, then the maximum fringe order at the point of failure would be 16. This is the same order observed for the 1-inch flat plate at failure. The foregoing

discussion indicates that in selecting the type of probe to measure foundation strengths, the type of contact employed by the moving wheel loading is a factor to be considered, at least in the case of gelatin foundations. It may also be a consideration for a soil foundation.

Model No. 3

58. Test Results. This model was tested with the moving wheel load, using the grit belt in contact with the gelatin surface. The following Table I gives measurements taken from the moving picture sequence of isochromatic fringe patterns for this model.

Table I

Measurements from Model No. 3,
Moving Wheel, Grit Belt

Run No.	Defl., in.	Max. Fringe Order	Forward Speed of Wheel, in./sec.	Slip, %	Gelatin Differential, in.
1,2	0.6	7	3.0	0	0.3
3,4	0.6	7	2.5	0	0.3
5	0.6	7	1.4	0	0.3
6,7	0.6	6-7	2.5	+25	0.1
8	0.6	6-7	1.4	+25	0.1
9	0.6	6-7	1.6	+25	0.1

The grit belt provided a smooth contact surface against the gelatin, and no stress concentration is present at the wheel contact with the gelatin. For Run Nos. 1 through 5, with the wheel at 0 slip, the isochromatic stress pattern remained quite uniform. It differed from the pattern for static loading with the circular probe in that it was not symmetrical about the vertical axis of the wheel. Actually, the area of the maximum fringe value was displaced slightly ahead of the advancing wheel. For Run

Nos. 6 through 9, at +25% slip, the area of maximum fringe value was displaced slightly to the rear of the wheel. The maximum fringe order for the +25% slip appeared to vary from 6 to 7 during the run. Much of this variation may be attributed to surface marring that developed due to repeated passages of the wheel over the surface.

59. Discussion. The isochromatic pattern for the moving wheel loading was similar to that of the semicircular probe loaded statically, except that it was not symmetrical about the vertical axis. Another difference was that the semicircular probe at 0.6 inches deflection developed a maximum fringe order of about 5 (see Figure 23); whereas the moving wheel load developed approximately 7 fringes for this same deflection for both slips. This is a clear indication that for these moving wheel load conditions the maximum shear stress is greater than for the static load condition. It may also be seen from Table I that the maximum fringe order remained the same for a given load condition regardless of the forward speed of the wheel. This is to be expected since the deflection is held constant throughout the runs by the method of applying load. Gelatin differential is about one third as much for +25% slip as for 0 slip (see Table I).

Model No. 4

60. Test Results. This model provided a study of the isoclinic development in the gelatin foundation under the moving wheel load at 0, +25%, and +50% slip. Six runs are shown by the moving picture film for each percent of slip. The isoclinics are shown at 15° intervals for each case. The grit belt was used on the load wheel and the deflection for each case (% slip) was 0.6 inches. The forward speed of the wheel was 2.5 in./sec. for 0 slip, 1.7 in./sec. for +25% slip, and 1.2 in./sec. for +50% slip. The gelatin differential was 0.3 inches for 0 slip, and 0.1 inches for +25% slip. There was no gelatin differential for the +50% slip case. For ease of study and comparison, the complete isoclinic pattern for 0, +25%, and +50% slip is presented on Figures 17(b), 18(b), and 19(b) respectively. These isoclinic patterns were obtained by tracing the isoclinics recorded by the moving picture sequence for each slip. The motion pictures indicate little or no change in the position

of the isoclinic during each run.

61. Discussion. As would be expected, the isoclinic patterns shown on Figures 17(b), 18(b), and 19(b) are not symmetrical about the vertical axis of the wheel. For the case of 0 slip, they tend to bunch to the rear of the wheel at the contact surface; while for the case of +25% and +50% slip, the opposite is true. Some indication of the normal stress distribution on the wheel can be obtained by using the isoclinic patterns to draw the principal stress trajectories or isostatics. This has been done on Figures 17(c), 18(c), and 19(c). On Figure 17(c) (0 slip), the number of trajectories normal to the wheel contact is greatest to the rear of the wheel. This would indicate that the normal stress distribution on the wheel contact surface is greater on the portion of the wheel on the left side of its vertical axis, or the side away from the direction of movement. Figure 18(c) (+25% slip) indicates just the opposite; the normal stress distribution on the forward portion of the wheel is greater than that on the rear portion in contact with the foundation. This condition is more pronounced in Figure 19(c) (+50% slip). Thus, for +50% slip, the normal stress distribution on the forward contact surface of the wheel is greater than for +25% slip; and in both cases, the normal stress distribution on the aft contact surface is less than that on the forward portion of the contact surface.

Model No. 5

62. Test Results. This model, tested with the grit belt, was similar to Model Nos. 3 and 4, except that the wheel deflection used was 0.55 inches instead of 0.60 inches. As indicated in paragraph 42 e., the purpose of testing this model was to provide well-defined photographs of the isochromatic fringe pattern for the moving wheel load. These photographs for 0, +25%, and +50% slip are reproduced on Figures 17(a), 18(a), and 19(a) respectively. Figure 16(a) is a photograph of the isochromatic fringe pattern for the static loading of the wheel at the same deflection (0.55 inches) used for the moving wheel load. The difference in deflection between this model and the models recorded on motion picture film does not affect the location of the isoclinics; and will not affect the

overall results. The following Table J summarizes the pertinent measurements and results for this model.

Table J

Measurements for Model No. 5 - Moving Wheel, Grit Belt

Loading Condition	Slip, %	Defl., in.	Max. Fringe Order	Forward Speed of Wheel, in./sec.
Wheel Static	--	0.55	5.0	0
Wheel Moving	0	0.55	7.0	4.0
Wheel Moving	+25	0.55	6.0	3.0
Wheel Moving	+50	0.55	6.0	2.0

63. Discussion. Table J and the isochromatic fringe patterns of Figures 16(a), 17(a), 18(a), and 19(a) provide a good comparison of the stress variation for the static wheel load and the moving wheel load at the three slip conditions. The forward speed of the wheel does vary (see Table J) for the three degrees of slip. However, previous results (see Table I) indicate that there is no change in the stress pattern, even when the speed is doubled at the same degree of slip. The fact that the deflection is constant for each run, and the speeds are relatively slow, would not lead one to expect a change in the stress pattern because of a change in speed. Table J and the isochromatic patterns for the static and moving wheel loadings confirm more precisely the fact that the maximum fringe order or maximum shear stress is greater for the moving wheel loads than for the static loading; and that the maximum shear stress developed by the moving wheel at 0 slip is greater than at +25% and +50% slip. The total load for all runs should remain constant, since the gelatin is loaded to a constant set deflection by lowering the track assembly of the loading apparatus. In this case, at a deflection of 0.55 inches, a total load of 650 grams is indi ated by the curve of Figure 22. The shear

stress indicated by the maximum fringe order for the moving wheel load can be increased over that for the static wheel load by a change in normal stress distribution and by an increase in stress with constant total load. The discussion of paragraph 61 and the isostatic patterns of Figures 17(c), 18(c), and 19(c), clearly indicate a change in normal stress distribution at the moving wheel contact with the gelatin, as compared to that of the static case (see Figure 8(b)). An increase in stress could be caused by a decrease in the wheel contact area with the gelatin foundation. The contact area was measured for the three conditions of the moving wheel load and the static load. The results are given by the following Table K:

Table K

Unit Load Measurements for Model No. 5

Loading Condition	Slip, %	Total Load, lbs.	Wheel Contact Area, $in.^2$	Unit Load, psi
Wheel Static	-	1.43	1.93	0.74
Wheel Moving	0	1.43	1.75	0.82
Wheel Moving	+25	1.43	1.82	0.79
Wheel Moving	+50	1.43	1.82	0.79

The measurements in Table K are not precise; however, they do indicate the relative magnitude of the average contact stress for the four load conditions. Referring to Figure 10, wherein maximum fringe order is plotted against the unit loading for the semicircular probe as defined in Table K, it will be seen that for average contact stresses ranging from 0.74 to 0.82 psi, the maximum fringe value falls between 5 and 6. In Table J, the maximum fringe order for the static wheel load is 5; and for the moving wheel load at 0 slip, it is 7. Therefore, it appears reasonable to assume that the main factor causing the increase in the maximum

fringe order, (maximum shear stress) when the wheel load changes from a static position to a moving load at 0, +25%, and +50% slip, is the redistribution of normal stress at the wheel contact with the gelatin foundation. The matter of stress distribution is explored further by preparing Figures 16(d), 17(d), 18(d), and 19(d). These figures show the contours of equal shear stress on the vertical and horizontal planes in the gelatin foundation beneath the static wheel and the moving wheel at the three conditions of slip. They were obtained using the isochromatic fringe patterns of Model No. 5 (Figures 16(a), 17(a), 18(a), and 19(a)), and the isoclinic patterns of Model No. 4 (Figures 17(b), 18(b), and 19(b)). The symmetrical isoclinic pattern of Fig. 18(b) was used to obtain the τ_{xy} contours shown on Figure 16(d). The values for plotting the τ_{xy} contours were computed as described by equation (2) paragraph 5. Actual stresses in lbs./in.^{2} can be obtained by multiplying the fringe value given for the τ_{xy} contours by the model fringe calibration value, 2F, or 0.128 psi (see paragraph 5). The τ_{xy} contours for the static wheel load (Figure 16(d)) are of course symmetrical about the vertical axis of the wheel; and for the moving wheel load at the three degrees of slip (Figures 17(d), 18(d), and 19(d)), they are definitely unsymmetrical as would be expected. This dissymmetry for the moving wheel load i interesting in that the shear stress on the x and y planes in the gelatin foundation is greater beneath the forward portion of the wheel than beneath the aft portion for the moving wheel at 0 slip; while the opposite is true for the conditions of +25% and +50% slip. This is also true for the maximum shear stresses, but to a lesser degree. Figure 20 has been prepared from Figures 16(d), 17(d), 18(d), and 19(d) to illustrate this distribution of shear stress on a horizontal plane. This figure shows plots of shear stress distribution on a horizontal plane 0.25 inches below the point at which the vertical axis of the wheel intersects the gelatin surface for the case of the static wheel loading and of the moving wheel load at the three conditions of slip. The shear stress distribution for the static wheel load, shown on Figure 20, is symmetrical about the vertical axis of the wheel with a reversal in shear stress occurring where the horizontal plane intersects the 90° isoclinic, which for

this case coincides with the vertical axis of the wheel. This is to be expected, since all normal stresses are symmetrical about this axis. For the moving wheel load, the shear stress distributions are unbalanced, as are the normal stresses. For the case of 0 slip, the reversal in shear stress distribution is slightly behind the vertical axis of the wheel; and for the cases of +25% and +50% slip, the reversal is ahead of the vertical axis. For the last two cases the distance ahead of the vertical axis increases with the percentage of slip. The magnitude of the total shear force to the right and left of the point of reversal is shown in pounds on Figure 20. These values are for the 1-inch width of the model, and are obtained from the area below the curves of shear stress distribution multiplied by the model fringe value 2F or 0.128 lbs./in.^{2}. The absolute magnitude of the total shear force on the horizontal plane is appreciable, varying from about 40% to 50% of the total vertical load on the wheel. The chord length for the portion of the wheel in contact with the gelatin surface is also shown on Figure 20. The area of the contact surface is computed from the chord lengths, which are shown in their relative position with regard to the horizontal and vertical axis of the wheel. The chord is horizontal for the static wheel load. At 0 slip, the angle the chord makes with the horizontal is about 5.4°. This angle is about 3.4° for +25% slip, and 2.0° for +50% slip. There appears to be a definite relation between this angle and the percent of slip.

Summary and Discussion

Model Simulation of Moving Wheel on a Soil Foundation

64. The gelatin foundation loaded with the moving wheel has the following limitations when compared with this type of loading on a prototype soil foundation:

a. The strain conditions in the gelatin model are two-dimensional rather than three-dimensional, as in the case of a moving wheel loading on a soil foundation.

b. The deformation of the gelatin foundation is elastic in character, as compared to the more plastic deformation of a weak cohesive

soil. For the moving wheel load on the gelatin foundation, no permanent deformation of the gelatin surface takes place, and no bow wave develops ahead of the wheel.

c. A further limitation is the method of loading the moving wheel for the model. As described in paragraph 43, this is accomplished by lowering the entire apparatus so that the wheel applies a constant deformation to the gelatin foundation. In the case of a prototype loading, there would be acceleration effects on the load and its intensity would be affected by the speed of travel of the wheel.

Advantages and Application of the Photoelastic Model Studies

65. The photoelastic methods, procedural testing, and observational techniques developed as a part of this study offer the following advantages and applications:

a. Results of the tests are reproducible, and comparisons between the static and moving wheel load conditions can be made reliable on a quantitative basis.

b. Although there are certain limitations to applying the results of the model studies directly to prototype wheel loadings on a weak cohesive soil, the photoelastic results do indicate differences in stress conditions and stress distribution for different loading conditions of the static and moving wheel loads. These differences and their degree of differences should be helpful in planning and analyzing prototype tests.

c. The isoclinic and isochromatic patterns from Model Nos. 4 and 5 provide the necessary information for computing normal and shear stress distribution on selected planes in the models for the various loading conditions subject to the following limitations:

(1) Computations of normal and shear stress in the gelatin at the contact surface of the wheel are not practical since the isochromatic pattern is not sufficiently well defined in this area.

(2) The isochromatic patterns are sufficiently well defined at a distance of 0.25 inches or more from the wheel contact surface for reliable computations of normal and shear stress distribution.

(3) The quantitative reliability of normal and shear stress computations is dependent on the accuracy with which the normal and shear stress is defined at a given point where the computations are started. For example, computations are usually started at a free surface, where the stress normal to the surface is a principal stress and equal to zero. The other principal stress is obtained directly from the isochromatic fringe order (see paragraph 3). As may be seen from Figures 16(a), 17(a), 18(a), and 19(a), the fringe order at the free surface of the gelatin is not too well defined. Therefore, in future studies of this type, provisions should be made to define the normal stresses at not less than two points. This could be accomplished by encapsulated strain gages calibrated in the gelatin by a uniform surface loading.

(4) A static check of the normal and shear stress distribution will require some approximations in the case of the moving wheel load conditions. This comes about by the fact that although the total vertical load is reasonably well defined from the deflection measurements, the shear force applied to the gelatin for the three cases of slip is not accurately determined for these studies.

Relationship of Probe Tests to the Moving Wheel Tests

66. The tests with the semicircular probe (static loading) having the same diameter as the moving wheel indicate a maximum shear stress (maximum fringe order times F) of lesser magnitude than that for the moving wheel load for the three cases of slip, for the same deflection. This emphasizes, at least for studies such as these, the necessity of accurately defining the state of stress beneath the probe and the moving wheel. This would allow more precise comparisons of normal and shear stresses to be made. This would also permit the computation of normal and shear stresses on planes of failure assumed for a soil foundation for these load conditions.

Failure Conditions Under the Moving Wheel Load

67. Failure of the gelatin foundation was produced in only one test. These were the tests of Model No. 2 with the cog belt on the moving wheel

(see paragraph 56). In this instance, initial failure appeared to take place at the point of maximum shear stress. However, the protruding cogs on the surface of the moving wheel complicated the stress pattern at failure by creating concentrations of stress at the surface. The other model tests with the grit belt were not tested to failure. The maximum deflection for the grit belt models was 0.6 inches, while for the cog belt at initial failure the deflection was 1.2 inches and 1.5 inches for final failure. This does not define the failure condition particularly well. Further studies should be made with the grit-belt-clad moving wheel at loads that will produce failure in the gelatin foundation. However, it is realized, from the deflection producing failure for the semicircular probe and the moving wheel with the cog belt, that the moving grit-clad wheel deflections at failure can be greater than one half the wheel diameter. This is certainly a limiting consideration for the prototype; but in the case of the gelatin foundation deflections greater than one half the diameter of the wheel are considered justified for determining the failure characteristics of the gelatin under the action of the moving wheel load. This should better define failure conditions for the moving wheel loading.

Conclusions

68. Test procedures and techniques developed in the course of these studies provide a means of obtaining photoelastic stress patterns for moving wheel loads at controlled degrees of slip.

69. Sufficient information has been developed to compute normal and shear stress distribution on planes in the gelatin foundation within 0.25 inches of the contact surface between the moving wheel load and gelatin, if certain approximations are made (see paragraph 65).

70. Further development or exploration of measuring techniques is needed to accurately define the stress at a point at two or more selected locations in the model foundations. However, preliminary preparation for this developmental work should include computations of normal and shear

stress distribution for the static and moving wheel loads using the available results and making the necessary approximations.

71. Since many prototype tests have been made of towed wheels on soil foundations, it would probably be desirable to make further studies of the towed wheel with sufficient friction available to turn the wheels as it is pulled in contact with the gelatin surface. This will require some minor modification of the load apparatus.

72. Further information should be obtained using presently developed techniques to define failure conditions in the gelatin foundation for the moving wheel load at 0 slip.

73. The following are specific conclusions concerning the action of the static and moving wheel loads on the gelatin foundation:

a. There was an increase in maximum shear stress for the moving wheel load at 0, +25%, and +50% slip over that of an equivalent static wheel load.

b. This increase in maximum shear stress is due to a redistribution of normal stress at the wheel contact with the gelatin.

c. The maximum shear stress under the action of the moving wheel load is greater at 0 slip than at +25% or +50% slip.

REFERENCES

1. Frocht M. M., Photoelasticity Vol. I - John Wiley & Sons, Inc., 1941

2. Frocht M. M., Photoelasticity Vol. II - John Wiley & Sons, Inc., 1948

Table 1

Summary of Load, Deflection and Stress Data
For Model Probes

Type of Model Probe	Bearing Area, sq. in.	Preliminary Loading					Failure Loading				
		Total Load, gms	Unit Load, psi	Defl., in.	Max. Fringe Order, n	τ_{max}, psi	Total Load, gms	Unit Load, psi	Defl., in.	Max. Fringe Order, n	τ_{max}, psi
1-Inch Flat Plate	1.00	835	1.84	0.80	13	0.83	1246	2.75	0.95	16	1.02
2 1/2-Inch Flat Plate	2.50	2215	1.95	1.40	16	1.02	2715	2.40	1.60	18	1.15
5-Inch Flat Plate	5.00	2510	1.10	1.10	16	1.02	4920	2.16	2.00	22	1.41
2 1/2-Inch Rounded	2.85	1025	0.80	0.90	7	0.45	4125	3.19	2.30	17	1.09
30° Wedge	1.40	--	--	--	--	--	300	0.47	1.00	10	0.64
90° Wedge	1.42	--	--	--	--	--	670	1.04	0.60	15	0.96
Semicircular	2.80*	1280	1.00	1.00	8	0.48	5580	2.86	2.90	20	1.28
Toroidal	3.70	1280	0.77	1.00	7.5	0.48	--	--	--	--	--

* For Failure Loading, Bearing Area was 4.30 sq. in.

Table 2

Load - Deflection Data for Model Probes

1-inch Flat Plate			2 1/2-inch Flat Plate			5-inch Flat Plate			2 1/2-inch Rounded			Semicircular			
Load, psi	Defl., in.	Fringe Order, n	Load, psi	Defl., in.	Fringe Order, n	Load, psi	Defl., in.	Fringe Order, n	Load, psi	Defl., in.	Fringe Order, n	Load, psi	Defl., in.	Fringe Order, n	Area, $in.^2$
1.40	0.70	12	0.99	0.80	12	0.80	0.90	13	0.80	0.90	7	1.03	0.90	7	2.3
1.84	0.80	13	1.51	1.10	14	1.06	1.10	15	1.64	1.40	12	1.84	1.65	12	3.2
2.75	0.95	16	1.95	1.30	16	1.28	1.30	17	2.03	1.70	14	- *	1.90	13	- *
			2.40	1.60	18	1.50	1.50	18	2.42	1.90	15	- *	2.10	15	- *
						1.72	1.65	19	3.19	2.30	17	2.59	2.20	16	3.55
						1.81	1.70	20				- *	2.55	18	- *
						1.94	1.80	21				- *	2.75	19	- *
						2.16	2.00	22				2.86	2.90	20	4.3

* Load and Area not obtained for these deflections

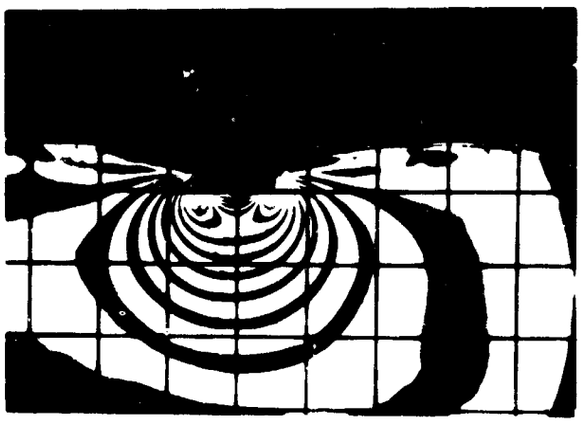

(a)

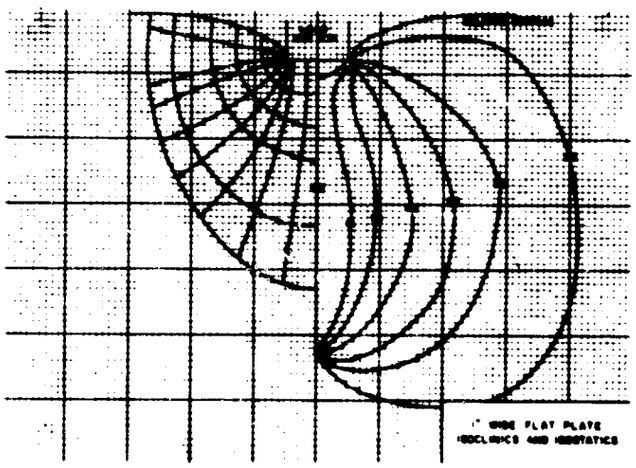

(b)

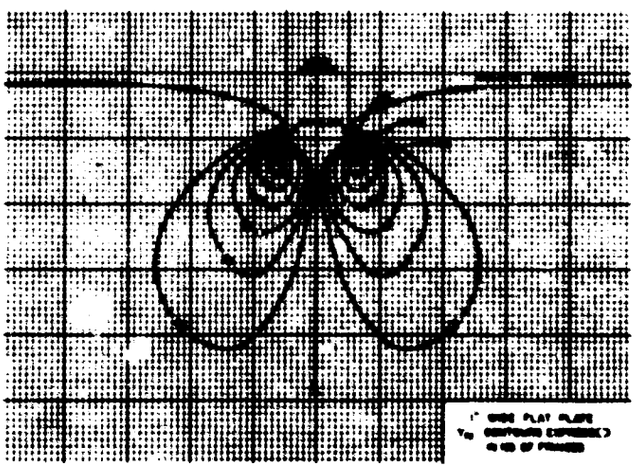

(c)

Figure 1. Isochromatics, isoclinics, isostatics, and τ_{xy} contours for 1-inch flat plate.

(a)

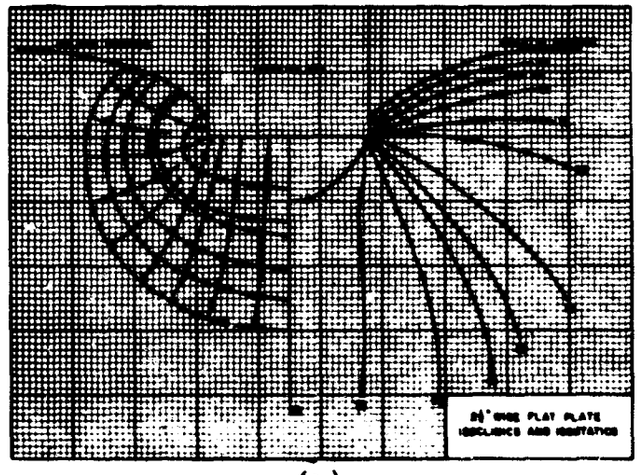

(b)

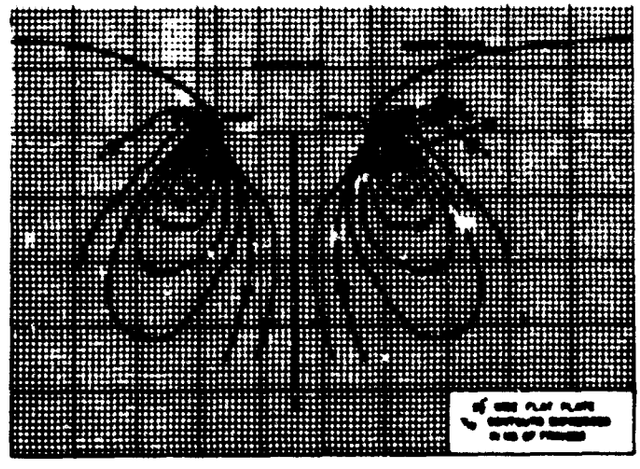

(c)

Figure 2. Isochromatics, isoclinics, isostatics, and τ_{xy} contours for 2 1/2-inch flat plate.

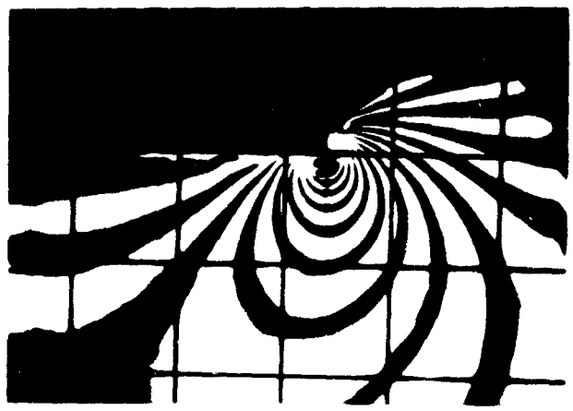

(a)

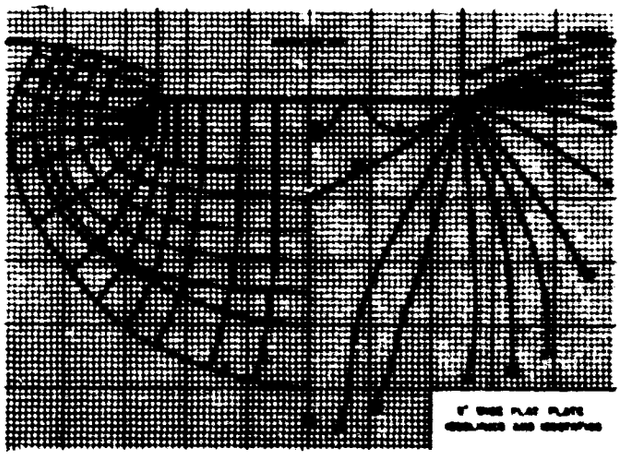

(b)

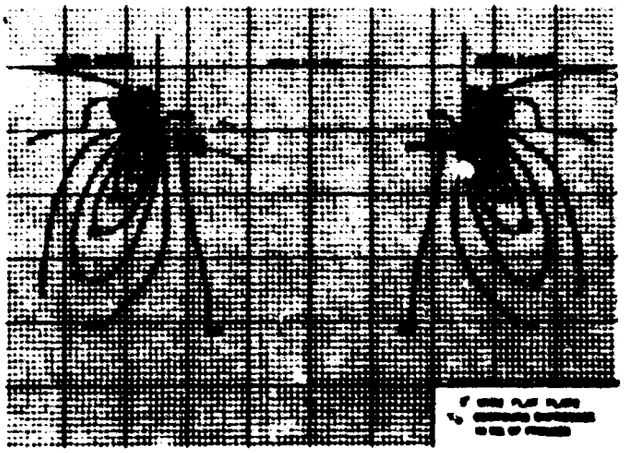

(c)

Figure 3. Isochromatics, isoclinics, isostatics, and τ_{xy} contours for 5-inch flat plate.

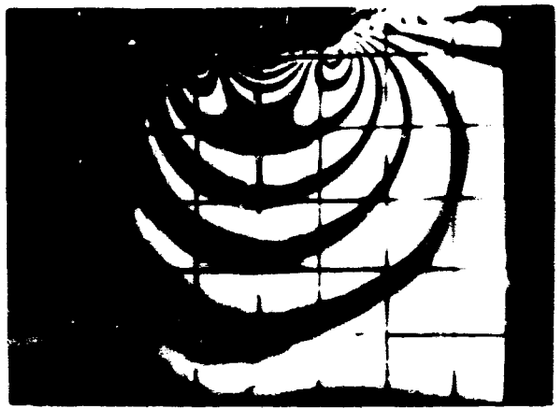

ISOCHROMATICS
2½" WIDE PLATE WITH ROUNDED EDGES

(a)

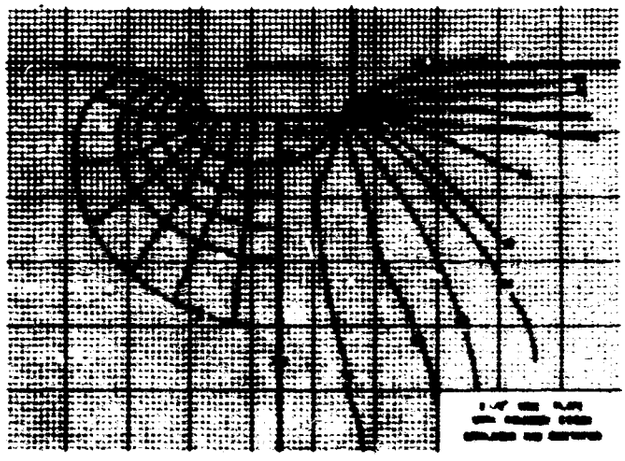

(b)

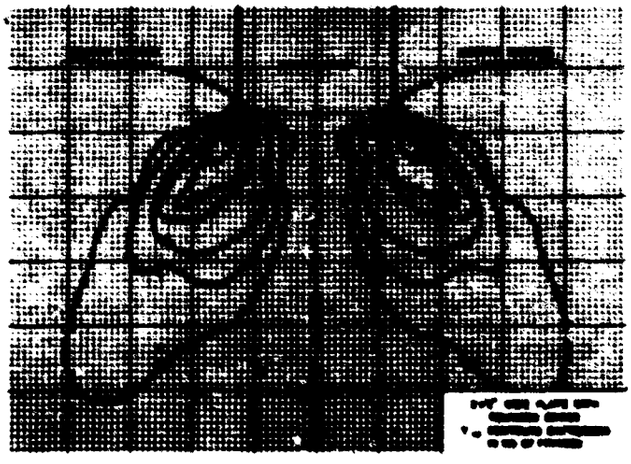

(c)

Figure 4. Isochromatics, isoclinics, isostatics, and τ_{xy} contours for 2 1/2-inch plate, rounded edges.

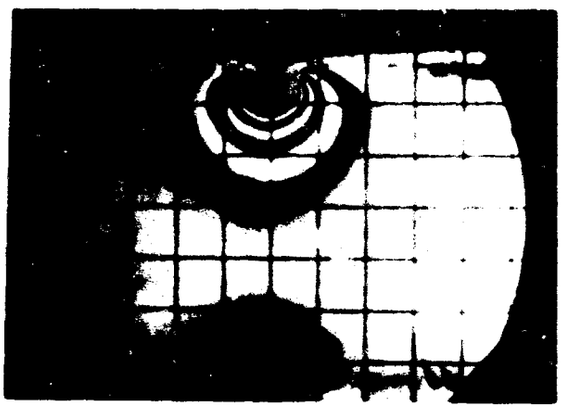

ISOCHROMATICS
30° WEDGE

(a)

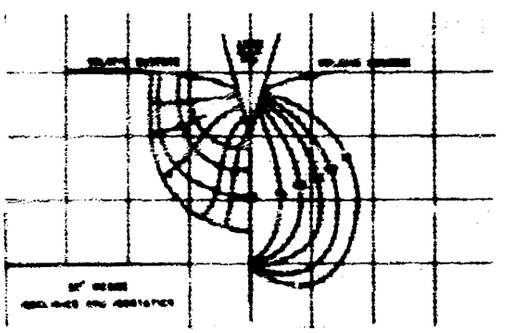

(b)

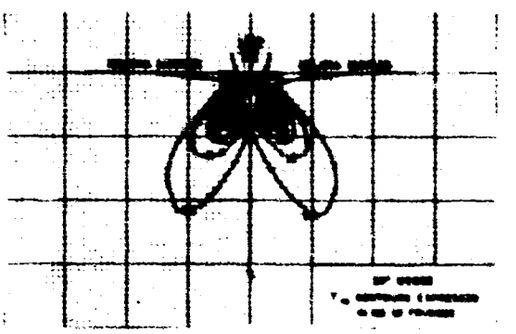

(c)

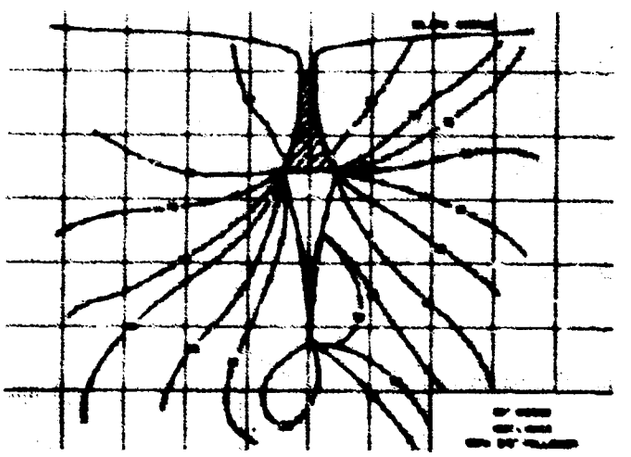

(d)

Figure 5. Isochromatics, isoclinics, isostatics, and τ_{xy} contours for 30° wedge; and isoclinics for 30° wedge with 3/8-inch follower

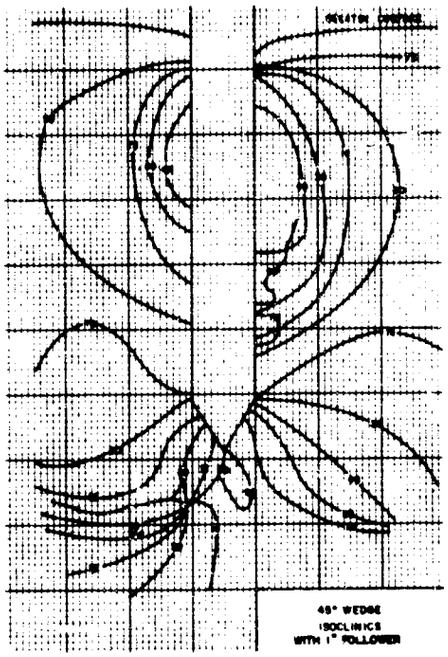

(b)

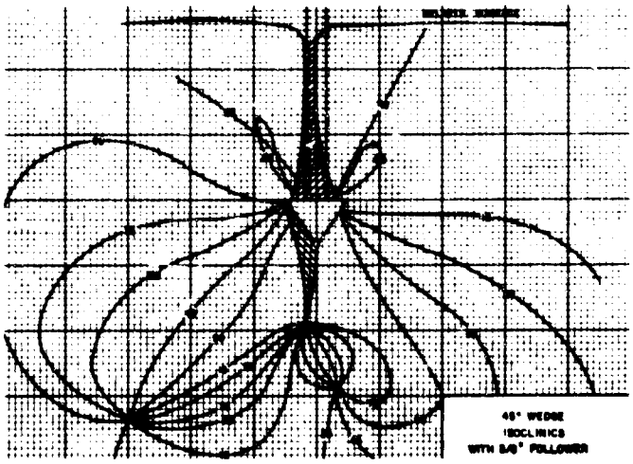

(c)

Figure 6. Isoclinics for 45° wedge with 3/8- and 1-inch followers.

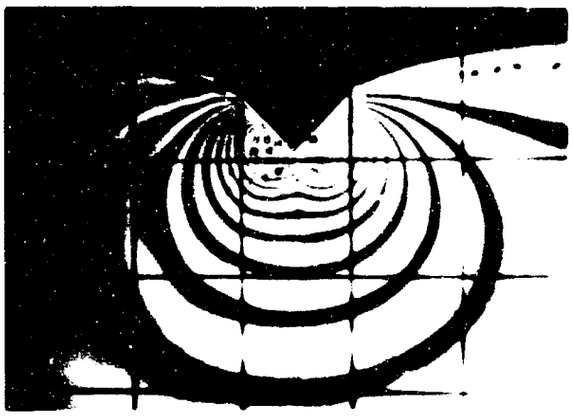

ISOCHROMATICS
90° WEDGE

(a)

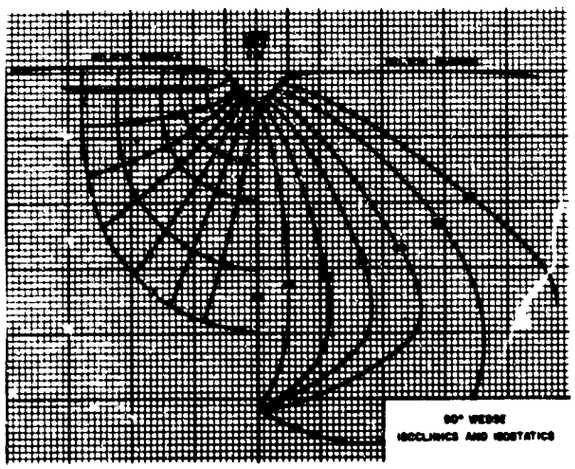

(b)

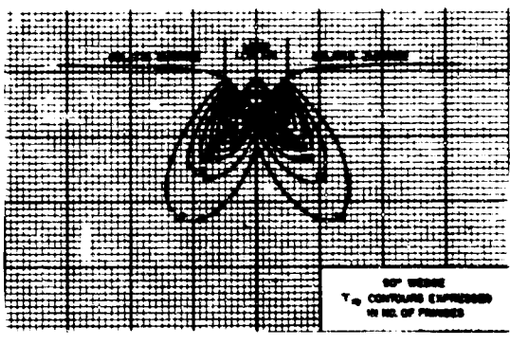

(c)

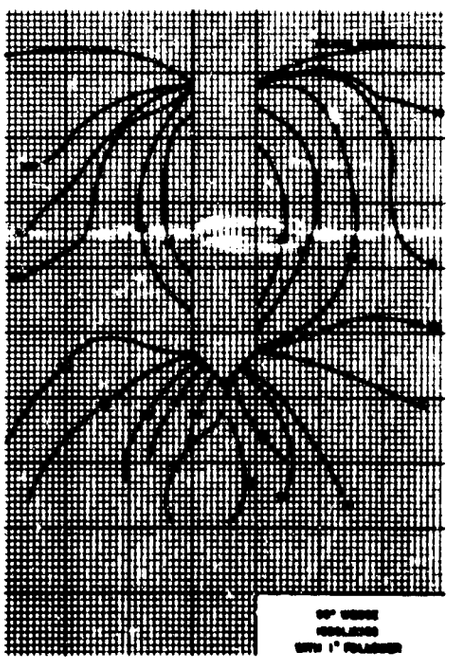

(d)

Figure 7. Isochromatics, isoclinics, isostatics, and τ_{xy} contours for 90° wedge; and isoclinics for 90° wedge with 1-inch follower.

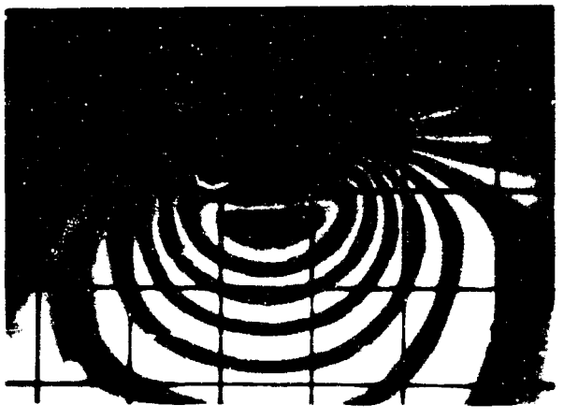

(a)

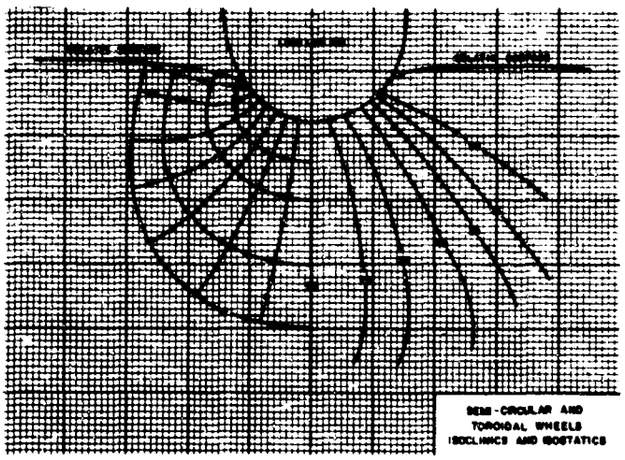

(b)

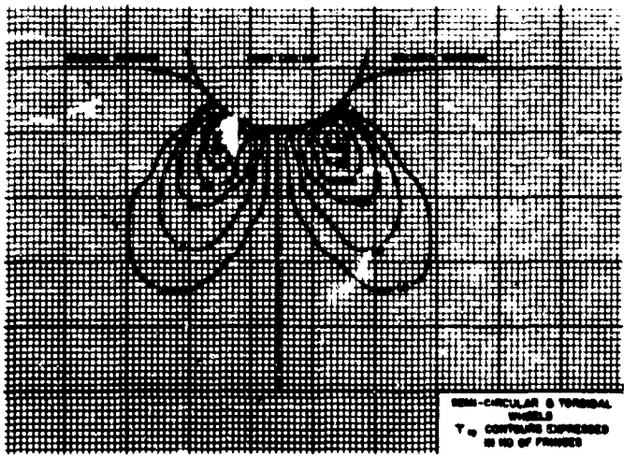

(c)

Figure 8. Isochromatics, isoclinics, isostatics, and τ_{xy} contours for semicircular and toroidal wheels.

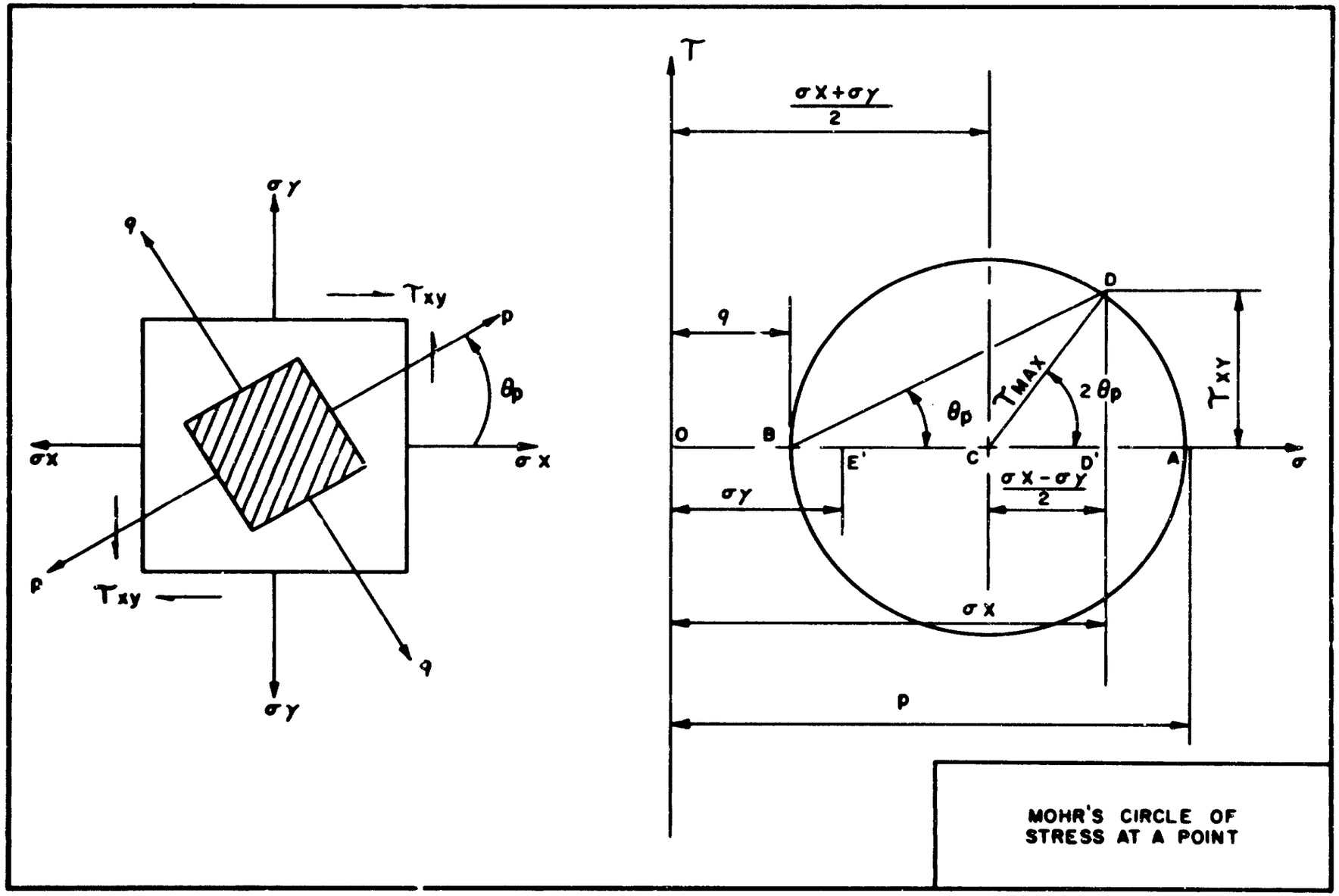

Figure 9. Graphical solution to finding stress at a point by Mohr's circle method.

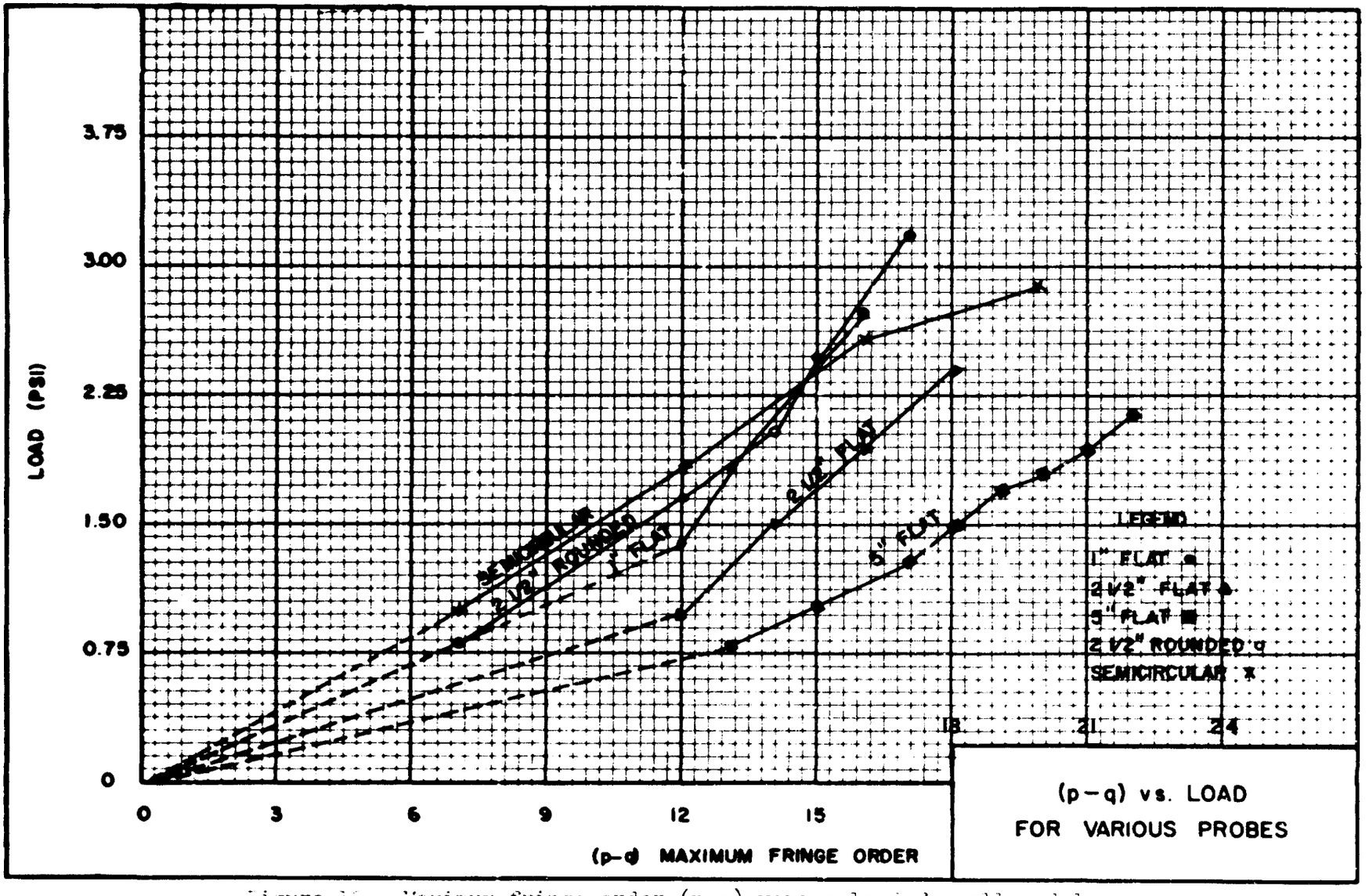

Figure 16. Maximum fringe order (p-q) versus load for all models.

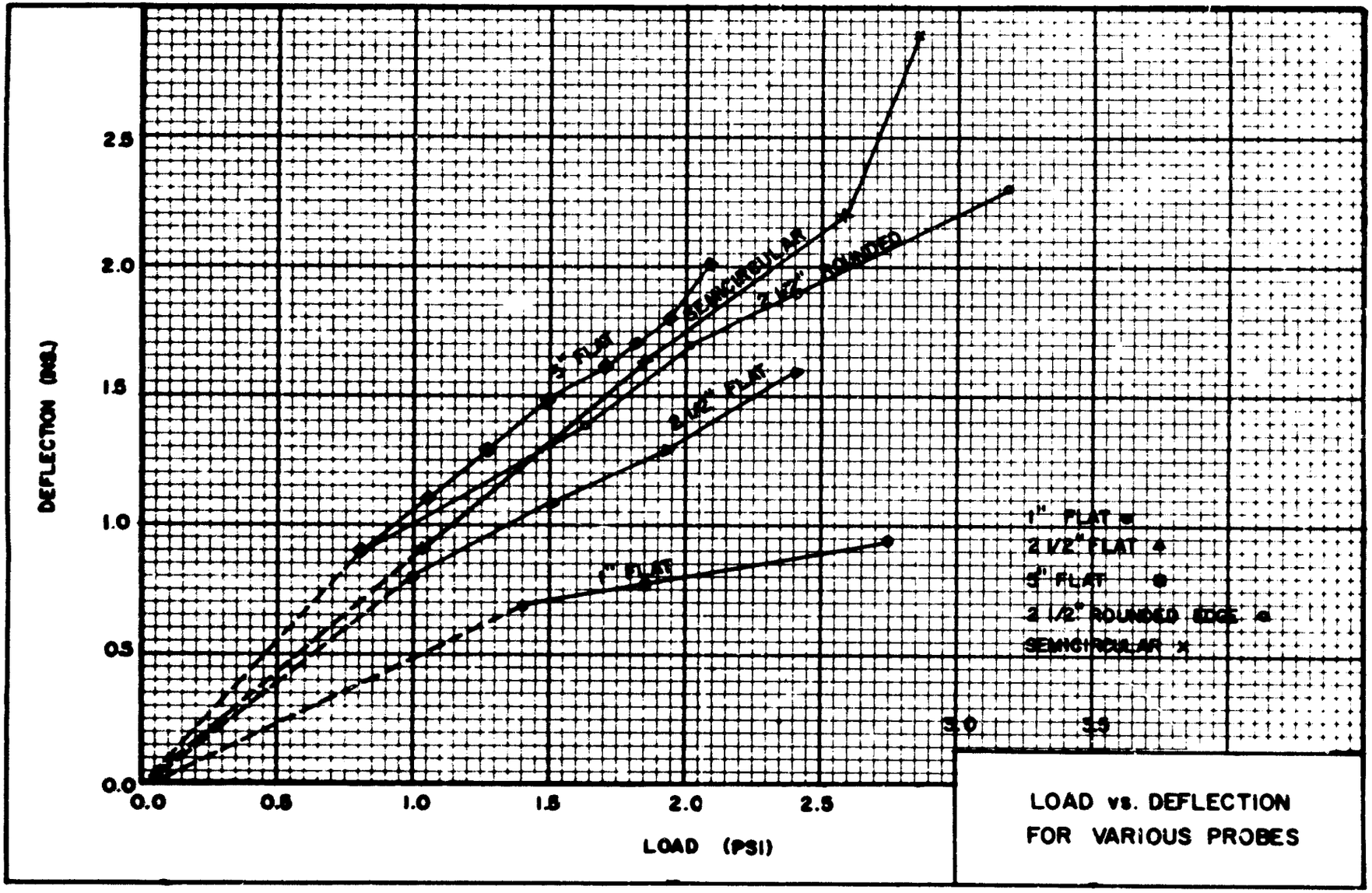

Figure 11. Load versus deflection for all models.

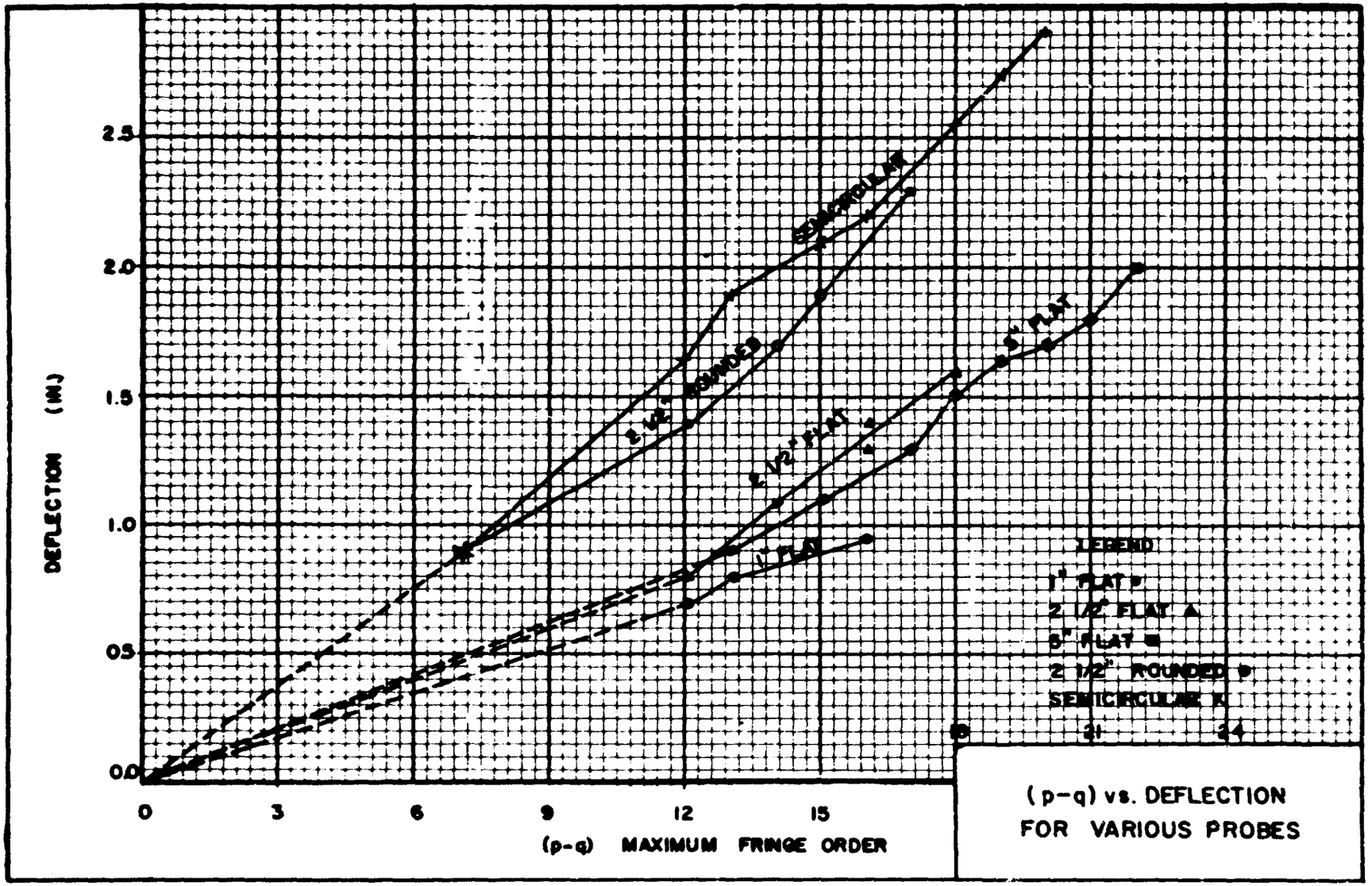

Figure 12. Maximum fringe order (p-q) versus deflection for all models.

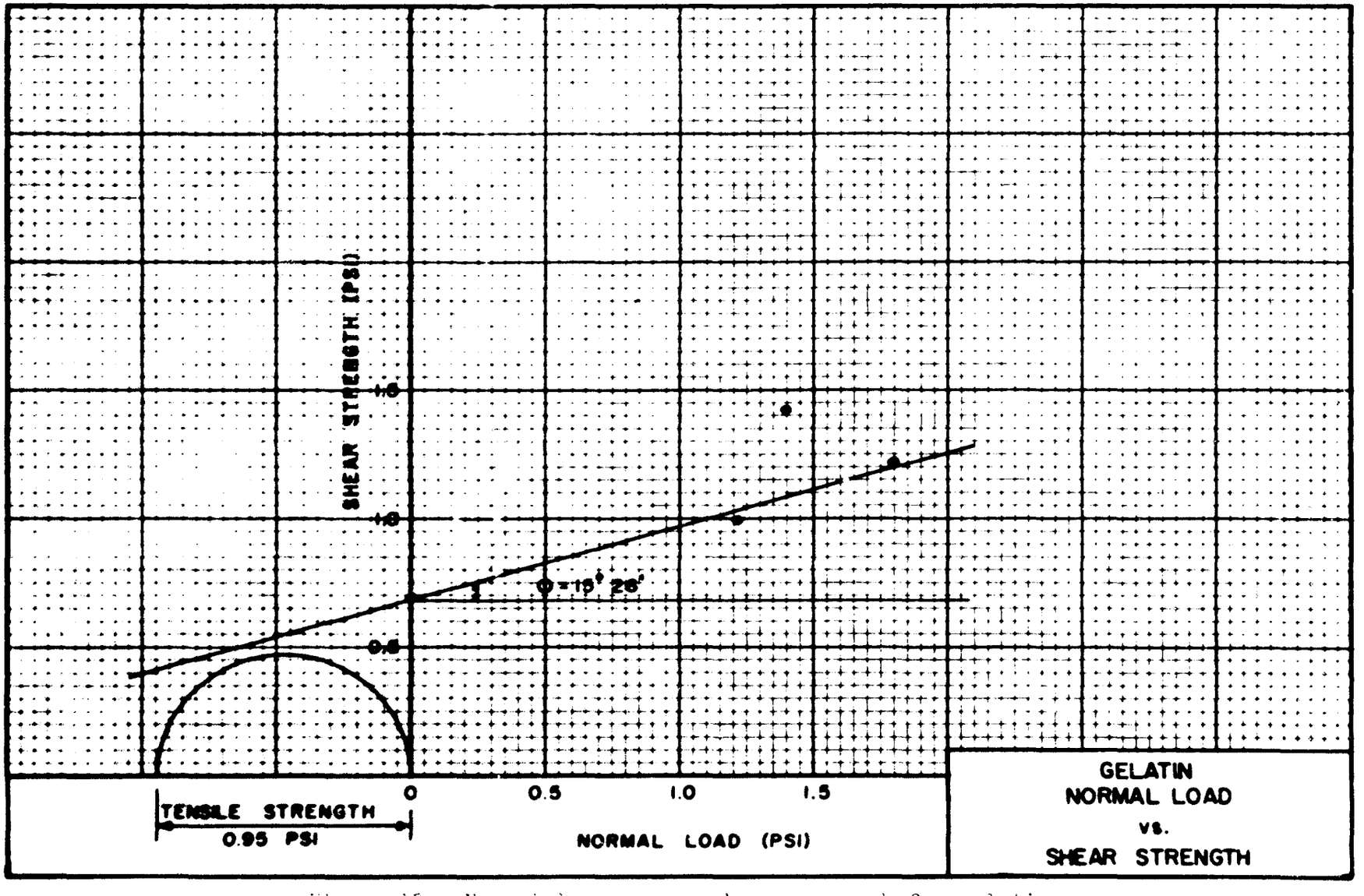

Figure 13. Normal load versus shear strength for gelatin.

(a) View of wheel and gear belt with track for moving wheel on gelatin surface.

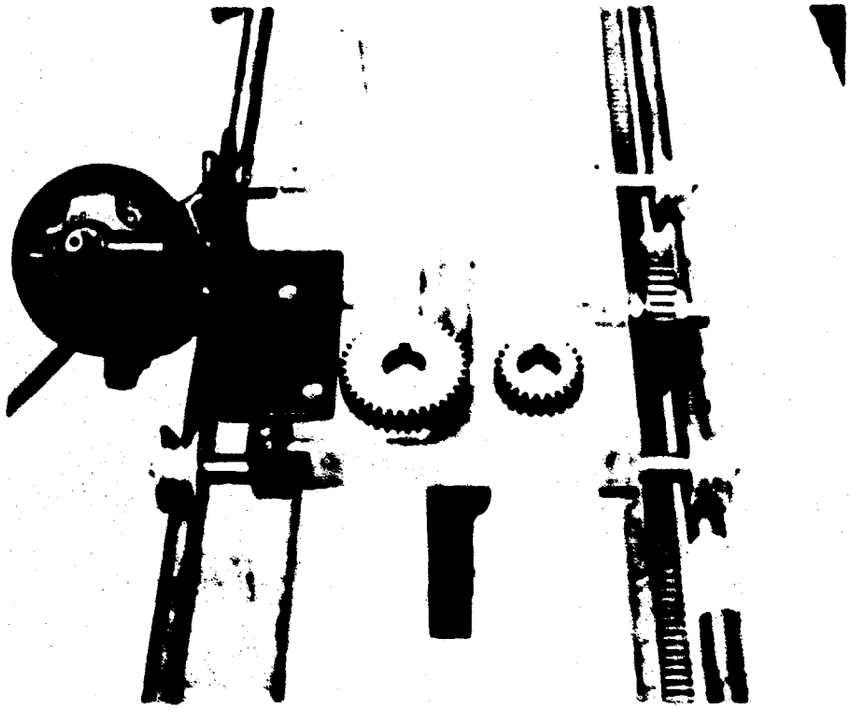

(b) Reduced speed motor with gear and rack arrangement and gears for +25% and +50% slip. Note the grit and thin timing belt.

Figure 14. Moving wheel apparatus and mounting track.

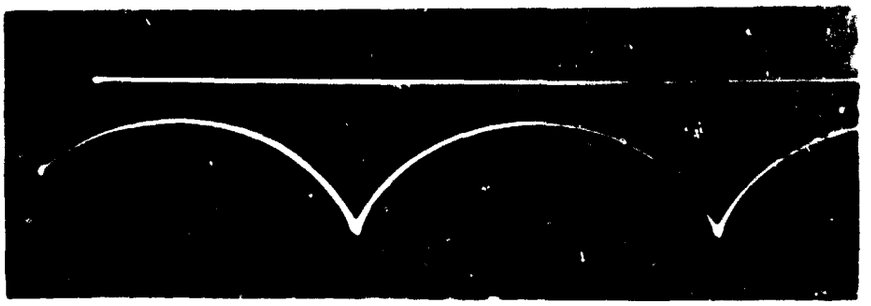

(a) Moving wheel cycloid for 0 slip.

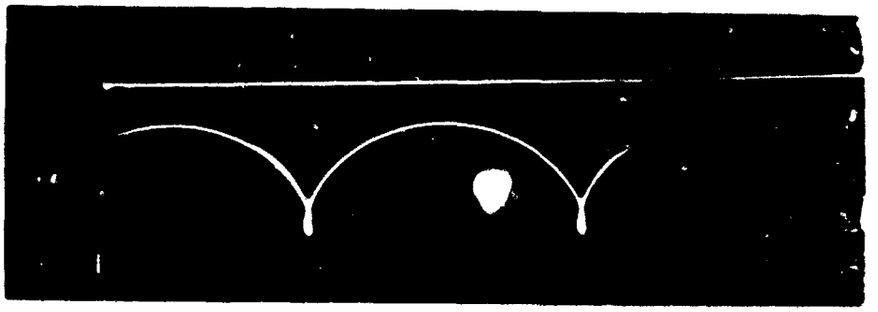

(b) Moving wheel cycloid for +25% slip.

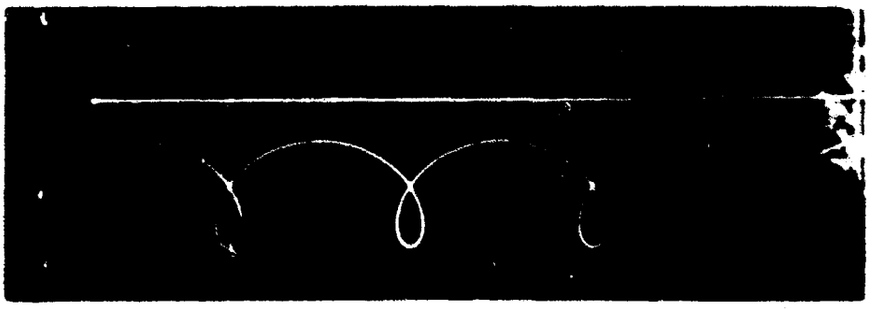

(c) Moving wheel cycloid for +50% slip.

Figure 15. Moving wheel cycloids at 0, +25%, and +50% slip.

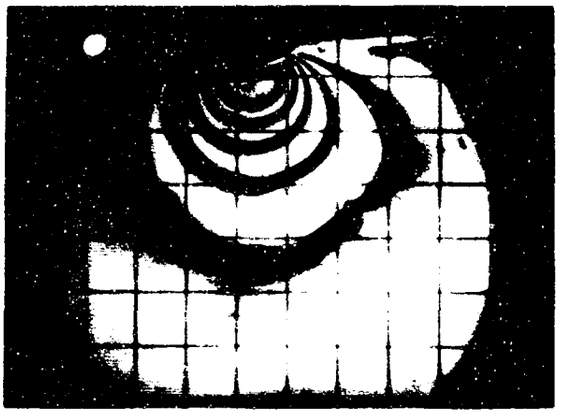

STATIC WHEEL
ISOCHROMATICS

(a)

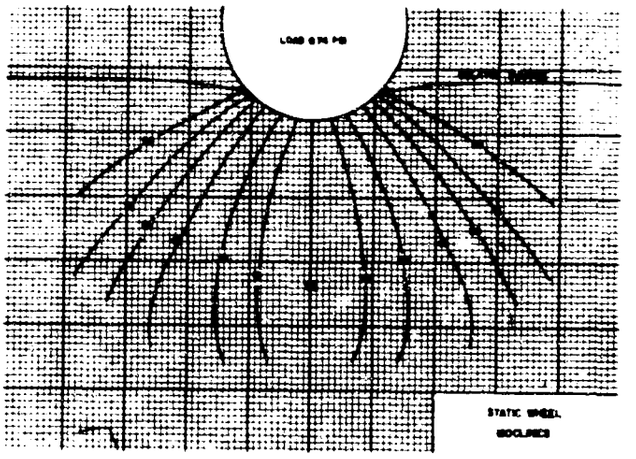

(b)

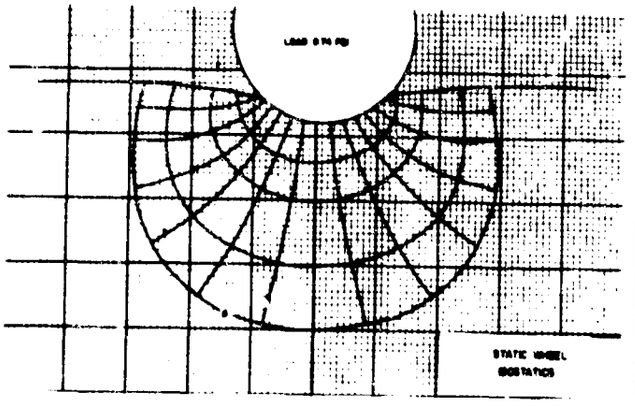

(c)

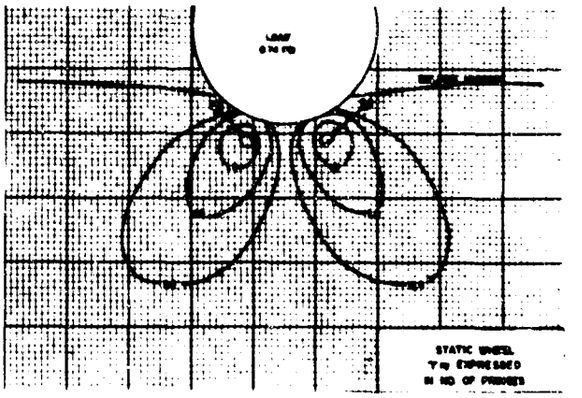

(d)

Figure 16. Isochromatics, isoclinics, isostatics, and τ_{xy} contours for static wheel.

(a)

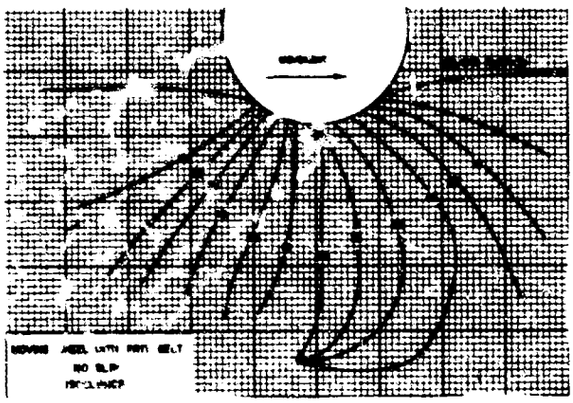

(b)

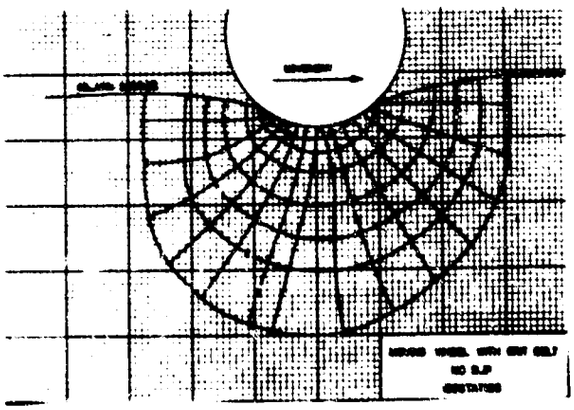

(c)

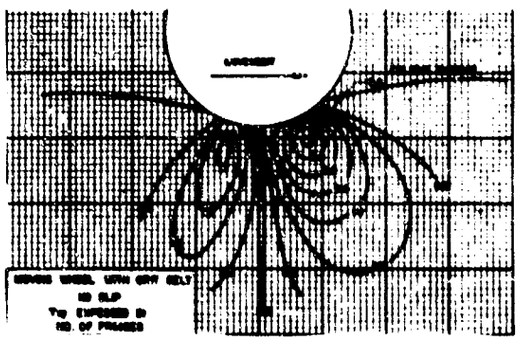

(d)

Figure 17. Isochromatics, isoclinics, isostatics, and τ_{xy} contours for moving wheel with grit belt, 0 slip.

(a)

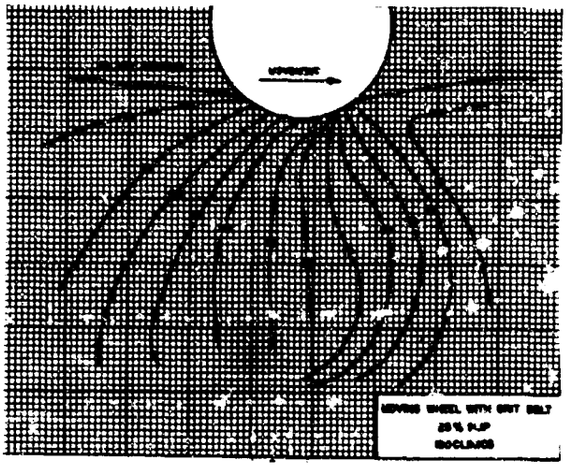

(b)

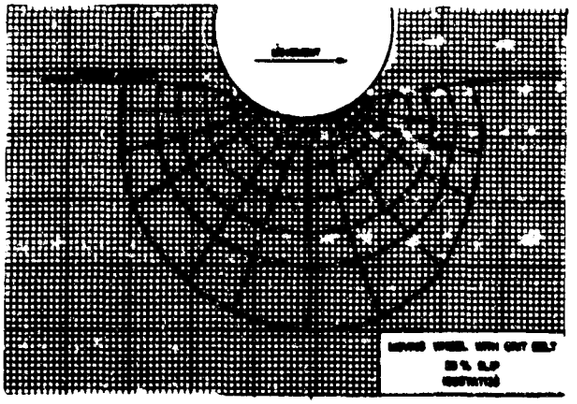

(c)

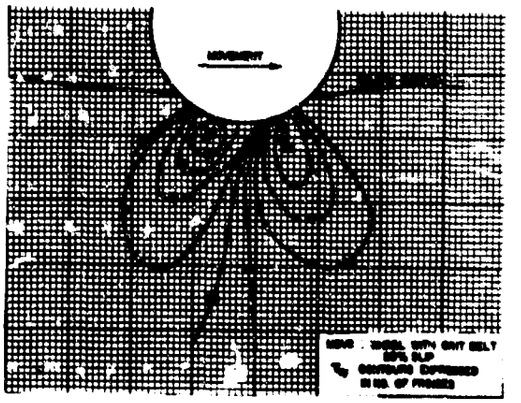

(d)

Figure 18. Isochromatics, isoclinics, isostatics, and τ_{xy} contours for moving wheel with grit belt, +25% slip.

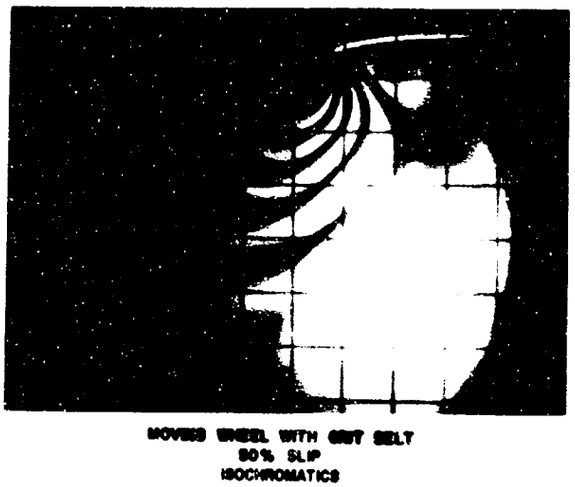

(a)

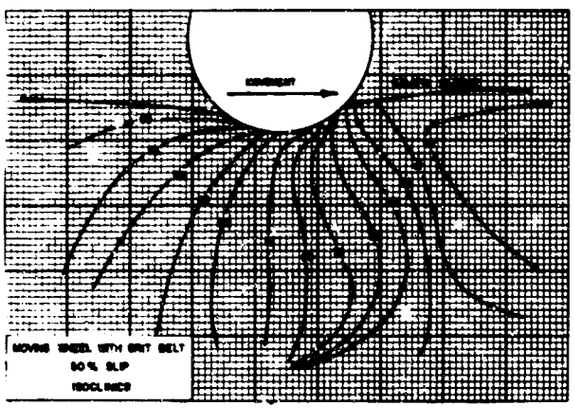

(b)

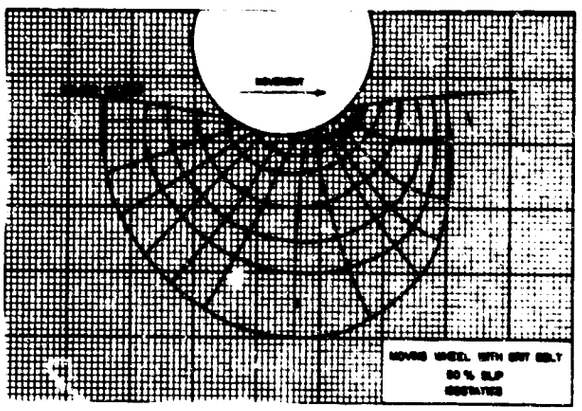

(c)

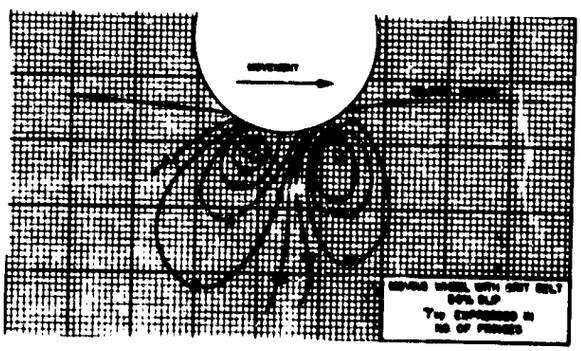

(d)

Figure 19. Isochromatics, isoclinics, isostatics, and τ_{xy} contours for moving wheel with grit belt, +50% slip.

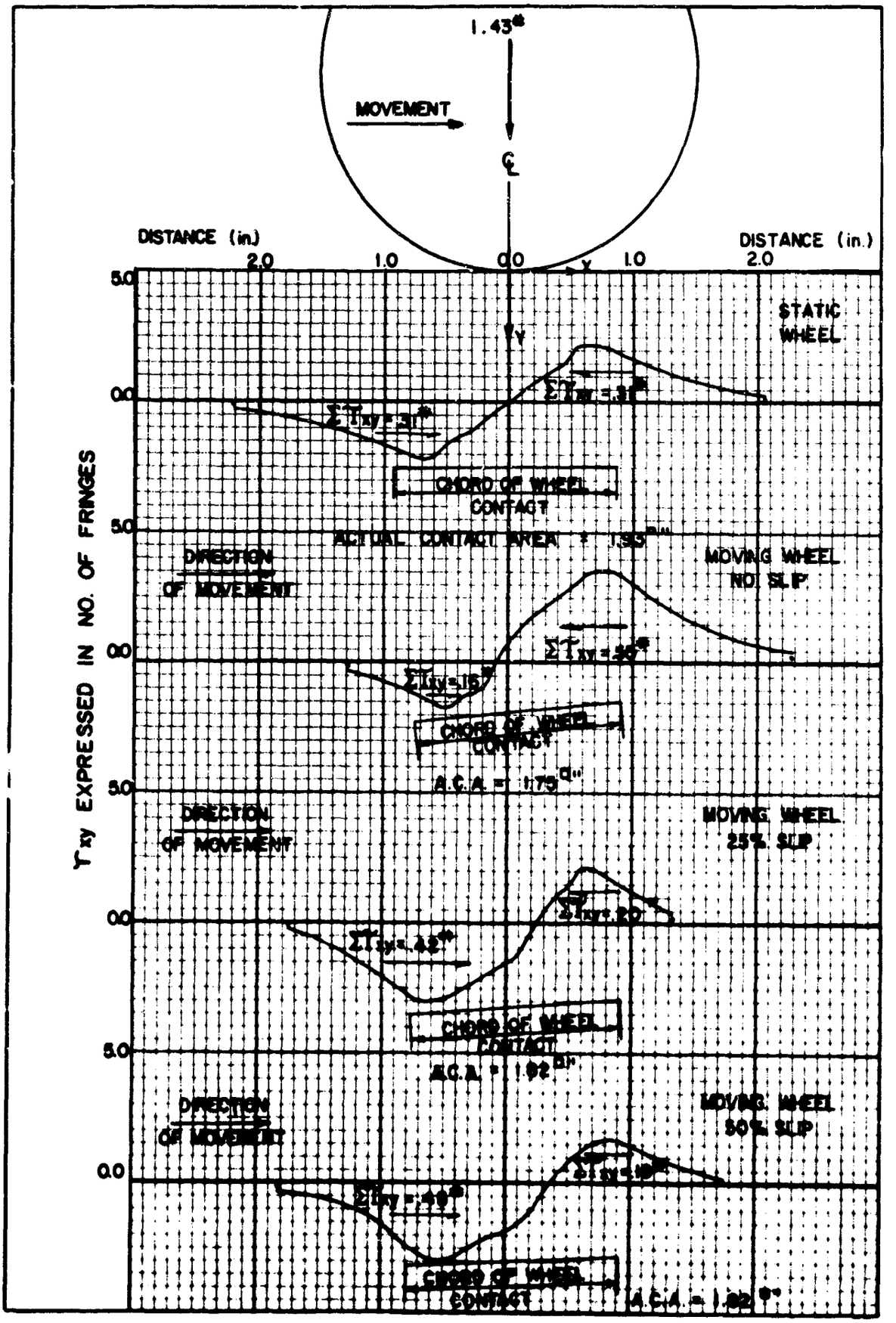

Figure 20. τ_{xy} versus distance from centerline of wheel on horizontal plane 0.25-inch below wheel contact.

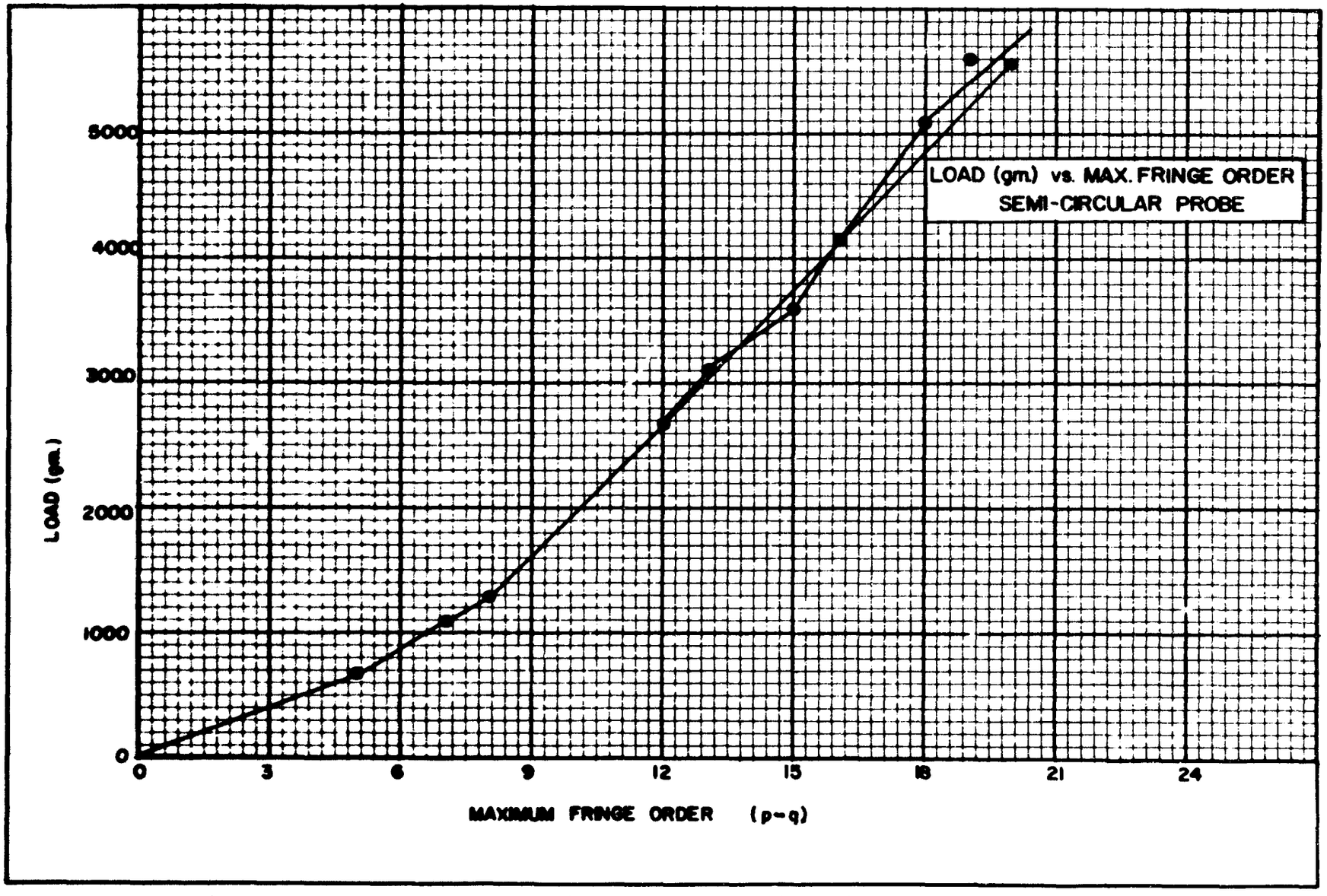

Figure 21. Maximum fringe order (p-q) versus load for semicircular probe.

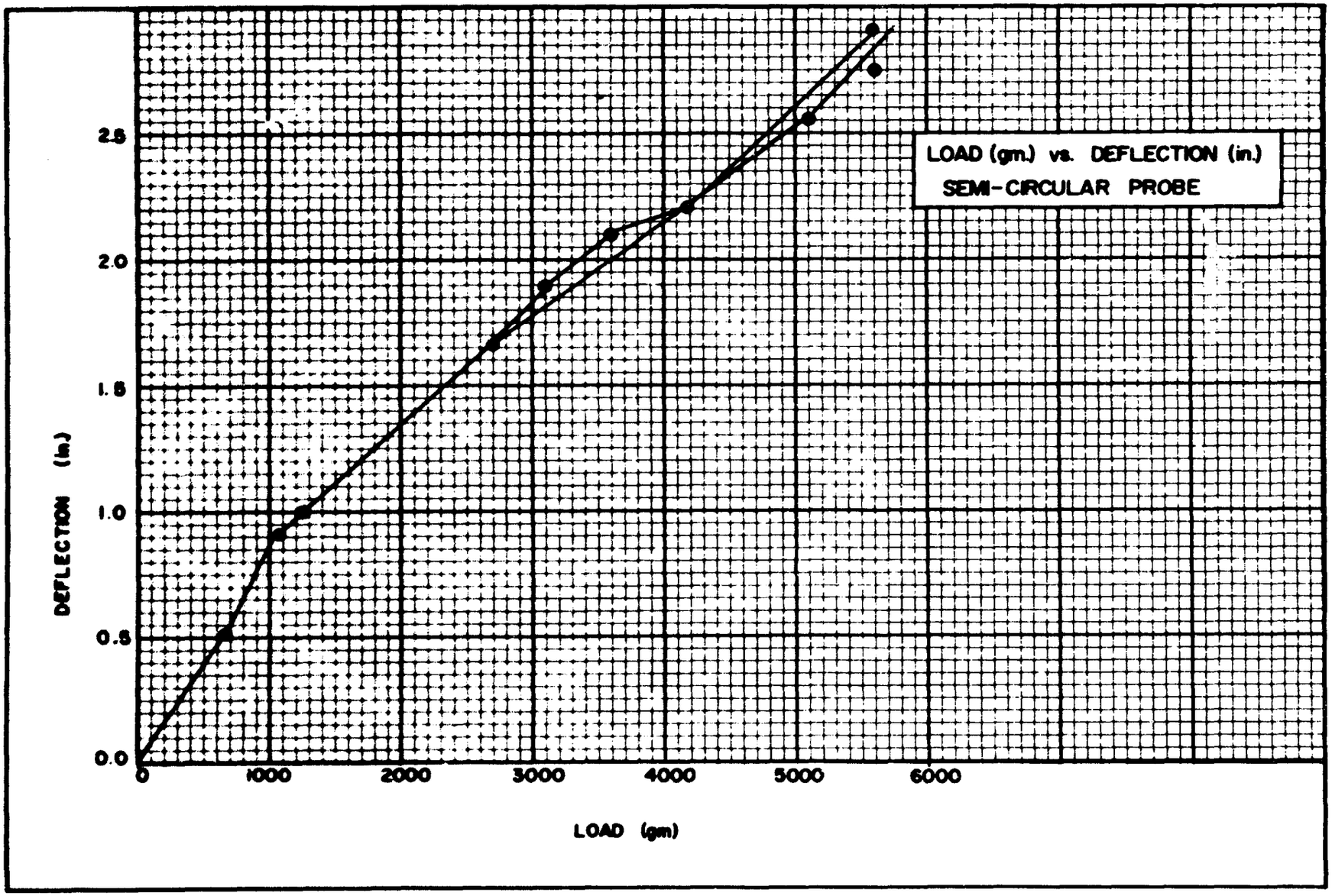

Figure 22. Load versus deflection for semicircular probe.

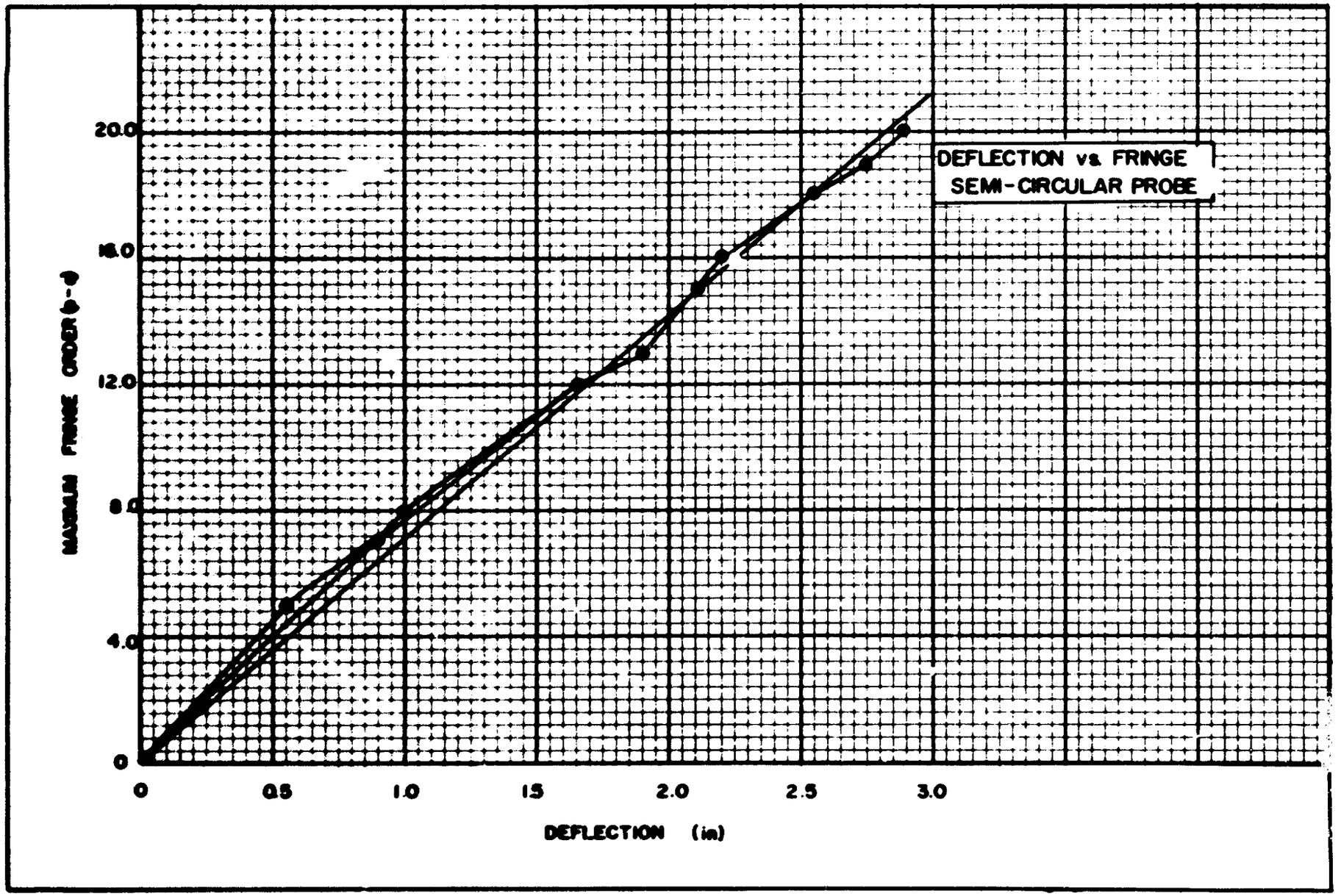

Figure 23. Maximum fringe order (p-q) versus deflection for semicircular probe.